Construction of artificial periosteum with methacrylamide gelatin hydrogel-wharton's jelly based on stem cell recruitment and its application in bone tissue engineering

Wentao Zhang [a,b,1], Tianze Sun [a,b,1], Jing Zhang [a,b], Xiantong Hu [d,e], Ming Yang [c], Liwei Han [d,e], Gang Xu [a,b], Yantao Zhao [d,e,**], Zhonghai Li [a,b,*]

[a] Department of Orthopaedics, First Affiliated Hospital of Dalian Medical University, Dalian, China
[b] Key Laboratory of Molecular Mechanism for Repair and Remodeling of Orthopaedic Diseases, Liaoning Province, China
[c] Department of Orthopedics, Southwest Hospital, Army Medical University, Chongqing, China
[d] Senior Department of Orthopaedics, The Fourth Medical Center of PLA General Hospital, Beijing, China
[e] Beijing Engineering Research Center of Orthopaedic Implants, Beijing, China

ARTICLE INFO

ABSTRACT

The presence of periosteum can greatly affect the repair of a bone fracture. An artificial periosteum imitates the biological function of natural periosteum, which is capable of protecting and maintaining bone tissue structure and promoting bone repair. In our artificial periosteum, biocompatible methacrylate gelatin was used to provide the mechanical support of the membrane, E7 peptide added bioactivity, and Wharton's jelly provided the biological activity support of the membrane, resulting in a hydrogel membrane (G-E-W) for the chemotactic recruitment of bone marrow mesenchymal stem cells (BMSCs) and promoting cell proliferation and osteogenic differentiation. In an in vitro experiment, the G-E-W membrane recruited BMSCs and promoted cell proliferation and osteogenic differentiation. After 4 weeks and 8 weeks of implantation in a rat skull defect, the group implanted with a G-E-W membrane was superior to the blank control group and single-component membrane group in both quantity and quality of new bone. The artificial G-E-W membrane recruits BMSC chemotaxis and promotes cell proliferation and osteogenic differentiation, thereby effectively improving the repair efficiency of fractures and bone defects.

1. Introduction

Bone fractures caused by accidental injury are commonly observed, with approximately 10–20% having delayed fracture healing. In severe cases, fracture nonunions and even disabilities can occur [1]. The repair of severe bone defects, especially critical defects, has always been a clinical challenge. Though success has been achieved with bone grafts of autologous, allogenic, and artificial substitutes, they are generally not efficient for repairing critical large segment bone defects [2–4]. Alternative solutions that can improve the efficiency and success rate of a critical bone defect repair are urgently required. Periosteum, which has a high degree of vascularization and serves as the reservoir of bone progenitor cells and growth factors, is a thin layer of connective tissue covering the surface of bone tissue. In cases of severe bone fracture, the periosteum is also damaged. Removal of the periosteum leads to slow osteogenesis or osteonecrosis of the bone defect [5,6] and fibrous tissue infiltration into the injured bone [7]; however, preservation of the periosteum or use of a periosteum tube graft significantly improves the bone graft incorporation and bone defect reconstruction [8,9]. The periosteum plays a key role in bone defect repair [10], which is largely ignored in current bone repair strategies. Studies have shown that the periosteum can release SDF-1/CXCR4 through paracrine and autocrine mechanisms during bone repair [11,12], playing an important role in the homing of mesenchymal stem cells (MSCs) [13]. Therefore, a bioengineered periosteum with stem cell homing ability may be significant for large bone defect repair. Instead of stem cell-based periosteum tissue

engineering, a cell-free engineering strategy harnessing cell homing is more practically applicable. In addition, reduced immune rejection and antibacterial ability are necessary for the bioengineered periosteum to repair complex bone defects.

Artificial periosteum can be divided into three types according to the bionic behavior: a cell sheet artificial periosteum, acellular scaffold artificial periosteum, and synthetic scaffold artificial periosteum (SSP) [10]. The preparation process of a cell sheet artificial periosteum is relatively simple, and it is combined with the technology of culturing target cells in vitro to induce various ECM components to form a complete healthy tissue slice [14]. This type of artificial periosteum involves some defects, such as invasive sampling, in vitro culture of seed cells, strict control of cell culture procedures, harsh culture conditions, and a long culture cycle [10]. Therefore, there are still many problems that need to be solved in preparing a cell sheet artificial periosteum. Regarding an acellular scaffold, the decellularization process removes the immunogenic components while retaining the natural effective components in the three-dimensional scaffold structure, which is a major source of membrane materials. However, the acellular process is complicated, and the antigenicity of the material can be effectively reduced by ensuring the complete removal of reagent consumables. At the same time, there is no effective method to remove non-collagen without affecting the collagen [10,15,16]. SSP can be divided into two categories: monolayer SSP and multilayer SSP, where both contains seed cells, bioactive factors, and scaffold materials [17–19]. Monolayer SSP avoids the interference of immunological problems; however, its flexibility and extensibility are not as good as those of a natural periosteum. Although the multilayer SSP that is similar to the natural periosteum in bionic structure can effectively make up for the deficiencies of a monolayer SSP, it will also be affected by many factors, such as the imitation of the multilayer structure in morphology but without a pore structure, the selection of bioactive factors, the influence of the internal environment on the biological behavior of materials, and the complicated preparation process of the composite membrane, all of which can affect the osteogenesis repair [10,18,20,21].

Methacrylated gelatin (GelMA) is an inexpensive photocrosslinkable hydrogel widely used in tissue engineering, which has the advantages of low immunogenicity, biocompatibility, and tissue adhesiveness because of multiple domains bindable to the cell surface receptors and extracellular matrix (ECM) proteins. ECM offers several biochemical cues that can be found in native tissues and has biochemical properties tunable by changing the concentration of the polymer, the degree of acidification, and the intensity of ultraviolet light during cross-linking [22]. The GelMA constructs formed by UV crosslinking show stability at physiological temperature. Recently, GelMA has been applied to periosteum engineering [23,24]. However, GelMA lacks adequate bioactivity, requiring further improvement.

Wharton's jelly (WJ), the human tissue surrounding umbilical cord blood vessels, contains few cells, numerous ECM components, such as collagen (COL), hyaluronic acid (HA), a variety of sulfated proteoglycans [25,26], and various growth factors such as epidermal growth factor (EGF), basic fibroblast growth factor (bFGF), platelet derived growth factor (PDGF), and transforming growth factor-β (TGF-β) [27]. WJ has characteristics of antibacterial ability, anti-inflammatory capability, biocompatibility, low immunogenicity, and no ethical controversies [28–32]. Therefore, WJ microparticles may be used to improve the bioactivity of GelMA for periosteum engineering.

E7 peptide, a short peptide with the amino acid sequence of "EPLQLKM", has a high specific affinity for MSCs and can improve their adhesion, proliferation, and migration [33]. Compared with functional proteins, functional short peptides are more resistant to pH and thermal changes, they are cost effective, controllable, and have less manufacturing cost and purification time [34,35]. E7 peptide has been used on biomaterials for MSCs homing [36], and the selective capture of MSCs over fibroblasts and immune cells by E7 peptide conjugated biomaterials has been reported [37]. Numerous studies have confirmed that E7 peptide plays a significant role in anchoring and recruiting BMSCs in vitro and in vivo [35,38–40]. In this study, a hydrogel artificial periosteum comprising GelMA, methacrylic anhydride (MA) treated WJ (WJMA) microparticles, and E7 peptide was developed to chemotactically recruit bone marrow mesenchymal stem cells (BMSCs) and promote cell proliferation and osteogenic differentiation to assist in the repair of large bone defects. GelMA functions to reconstruct the structure of the periosteum and provide the strength support of the artificial periosteum. The WJMA microparticles were used to improve the bioactivity. E7 peptide was used for MSC homing. The physical and mechanical properties of the bioengineered artificial periosteum and its effect on the growth, viability, recruitment, and osteogenic differentiation of MSCs was studied. The potential of the hydrogel for critical-size bone defect repair in vivo was evaluated (Fig. 1).

2. Materials and methods

2.1. Preparation of the artificial periosteum membranes

2.1.1. Preparation of the WJMA microparticles

WJ was collected from patients that provided consent at Maternal and Child Health Hospital of Jiangxi Province (RE-GC-TY-032). Fresh, clinically safe umbilical cord was repeatedly washed with physiological saline to remove blood. Arteries and veins were physically removed, the soft tissue was cut into small pieces to obtain WJ, and the WJ was then cleaned by ultrasound. WJ was freeze dried (FD8-3a, SIM International Group Co., Ltd, USA), cut into 2 mm × 2 mm slices, and ground into microparticles smaller than 100 μm (N9548, Beijing Hoder Co., Ltd, Beijing). The WJ microparticles were immersed in 4% (v/v) MA (M102519, Shanghai Aladdin Biochemical Technology Co., Ltd, Shanghai) in phosphate buffer solution (PBS) [41], and incubated in a horizontal constant temperature shaker (ZWY-200B, Zhongyiguoke Technology Co., Ltd, Beijing) at 4 °C for 24 h. The generated WJMA was then collected with filter paper, washed repeatedly with PBS, and centrifuged. After dialyzing in an 8–14 kD dialysis bag (YA1072, Beijing Solarbio Science & Technology Co., Ltd, Beijing) for 48 h to remove residual MA, the WJMA microparticles were freeze dried.

2.1.2. Synthesis of the artificial periosteum membranes

GelMA (SP-BI-G01-4, SUNP Biotechnology Co., Ltd, Beijing) was dissolved in PBS to a concentration of 10% w/v, and then 0.1% w/v acylphosphinate photo-initiator (SP-BI-C02-2, SUNP Biotechnology Co., Ltd) was added. The prepared solution of 0.2 ml was added to each well of a 48-well cell culture plate (REF-3548, Costar Co., Ltd, USA) to obtain the pure GelMA (G) membrane. E7 peptide of (0.006 mg, C0724804, Beijing Scilight Biotechnology Co., Ltd, Beijing) was added to each well to obtain the GelMA-E7 (G-E) composite membrane. WJMA microparticles (10 mg) were added to each well to create the GelMA-WJMA (G-W) composite membrane. E7 peptide (0.006 mg) and WJMA microparticles (10 mg) were added to each well to create the GelMA-E7-WJMA (G-E-W) multicomponent membrane. The solution was exposed to an ultraviolet point light source (Ultradent product, 395–480 nm, 10.5 mm curing tip, SP 1650 mW/cm^2, Suzhou Yunhe Company, China) for 60 s to form the hydrogel membrane. The membranes were cleaned, freeze dried, and sterilized by irradiation.

2.2. Characterization of the artificial periosteum membranes

2.2.1. Fourier transform infrared spectrometer analysis

The WJ microparticles, WJMA microparticles, and G, G-E, G-W, and G-E-W membranes were dried. After adding potassium bromide (BrK, Sinopharm Chemical Reagent Co., Ltd, China) powder with a mass ratio 1:100, the materials were ground and subject to Fourier transform infrared spectrometry (FTIR, Nicolet Co., Ltd, USA) analysis at a resolution of 4 cm^{-1} over a scanning range of 400–4000 cm^{-1} [42].
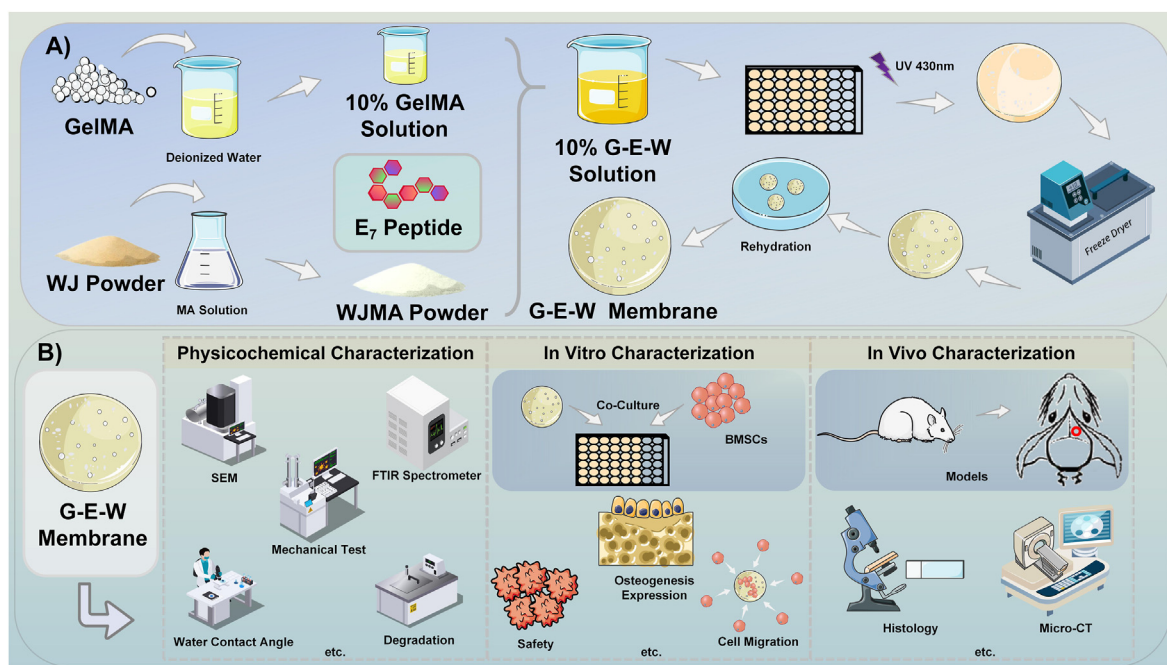
Fig. 1. Schematic diagram of the preparation and characterization of a G-E-W artificial periosteum for bone defect repair. A) The preparation process of the G-E-W artificial periosteum. B) Characterization of the physical and chemical properties, in vitro cell experiment and in vivo biocompatibility of the G-E-W artificial periosteum. BMSCs, bone marrow mesenchymal stem cells; GelMA, methacrylate gelatin; G-E-W, GelMA-E7-WJMA membrane; WJ, wharton's jelly; WJMA, WJ after methacrylic anhydride treatment; SEM, scanning electron microscope; UV, ultraviolet ray.

2.2.2. Macroscopic and microscopic structural observation

The G, G-E, G-W, and G-E-W membranes were freeze dried, placed on a uniform platform, and photographed by a digital camera (Canon EOS 80D, Canon Co., Ltd, China) to observe the color, appearance, and other characteristics. The membranes were fixed on the sample table with a conductive adhesive, sprayed with 7 nm gold (20 mA, 90 s), and imaged by scanning electron microscopy (SEM, SUPRA55, ZEISS Co., Ltd, Germany) to observe the microstructure of the materials [43].

2.2.3. Water contact angle

Membranes with a size of 1 cm × 1 cm were placed on the sample table for water contact angle measurement (JC2000DM, ZYKX, Beijing). A charge-coupled camera was used to capture the images of the liquid droplets, and the built-in software was used to analyze the water contact angle results (five samples for each membrane).

2.2.4. Swelling

After weighing the freeze-dried membranes (weight denoted as WD), they were placed in 20 ml PBS to carry out the rehydration experiment at 37 °C. At the time points of 0.25, 1, 2, 24, 24, and 48 h, the samples were obtained and weighed after removing surface water (weight denoted as WS). The swelling degree of the material was calculated as (WS − WD)/WD × 100% [44].

2.2.5. Mechanical testing

A universal testing machine (Testometric Co., Ltd, United Kingdom) was used to analyze the tensile strength of the membranes. The freeze-dried membranes were rehydrated for 4 h, then cut into the shape of 1 cm × 2 cm, stabilized by the clamps, and then stretched at a constant speed of 4 mm min^{-1} in the longitudinal direction until broken. The maximum load and deformation were recorded by the built-in software, and the maximum tensile force and tensile modulus were calculated (six samples for each membrane).

2.2.6. Degradation

First, the membranes were soaked in PBS at 37 °C for 4 h to reach the swelling equilibrium. After drying the surface, the membranes were weighed to record its initial mass (denoted as WO). The samples were then immersed in the prepared simulated body fluid and oscillated slightly at 37 °C. At the predetermined time points of 2, 4, 6, 8, 10, 12, 14, 16, 18, 20, 22, 24, 26, 28, 30, 32, 34, and 36 days, the membranes were retrieved to measure the remaining mass of the membranes (denoted as WT) after drying the surface, and then the membranes were re-immersed in fresh simulated body fluid. The degradation rate of the material was calculated as (WO − WT)/WO × 100% [41]. The pH value of the simulated body fluid in the degradation experiment was also monitored at each time point.

2.2.7. Stability of the E7 peptide in the membranes

Fluorescent E7 peptide (C0868404, Beijing Scilight Biotechnology Co., Ltd) was used to prepare the G-E and G-E-W membranes. The following procedures were conducted in the dark. After freeze drying, the materials were soaked in PBS at 37 °C for 4 h to reach the swelling equilibrium. The materials were then incubated in simulated body fluid and placed in a horizontal constant temperature shaker at 37 °C. At the predesignated time points of 1, 3, 5, and 7 days, the fluorescence signal was captured by fluorescence electron microscopy (IX-2-UCB-2, OLYMPUS CORPORATION Co., Ltd, Tokyo). At the same time, the fluorescence intensity of the solution at different predesignated time points was monitored by a multifunctional enzyme-labeled instrument (Varioskan LUX, Thermo Fisher Scientific Inc., China), and a standard curve was prepared to evaluate the content of fluorescent E7 peptide released from the membranes into the simulated body fluid. Finally, the content was plotted as a percentage of the initial fluorescent E7 peptide [39].

2.3. In vitro studies

2.3.1. Biocompatibility

A cell counting kit-8 (CCK-8) assay was used to detect the cytotoxicity of the membranes. After rehydrating the membranes with a complete culture medium of 89% Dulbecco's modified Eagle's medium (DMEM,

69,010,395, Beijing Labgic Technology Co., Ltd, Beijing), 10% fetal bovine serum (FBS, A4766801, Thermo Fisher Scientific Inc.), and 1% double antibody (J0408050, M&C GENE Technology, Ltd, Beijing) for 4 h, the leaching solution was prepared according to the existing leaching solution preparation standard ISO 10993–12 (GBT16882.12) with the complete culture medium as the solvent. L929 cells (CL0339, Fenghuishengwu Co., Ltd, China) were inoculated in a 96-well cell culture plate (REF-3599, Costar Co., Ltd) with 5×10^3 cells in 100 μl culture medium per well. The outer ring space of the cell culture plate was filled with PBS. After keeping at 37 °C and 5% carbon dioxide (CO_2) for 24 h, the culture medium was changed to the leaching solution. The cell medium was changed every 2 days. After culturing with the leaching solution for 1, 3, and 5 days, the CCK-8 reagent (SP-BI-C02-2, SUNP Biotechnology Co., Ltd) was used to measure the optical density (OD) at 450 nm using an enzyme-labeling instrument (357–808025, Thermo Fisher Scientific Inc.). The results of the cytotoxicity experiment were represented by the relative growth rate = (experimental group − blank group)/(control group − blank group).

2.3.2. Cell proliferation and viability staining

The CCK-8 assay was also used to detect the cell proliferation. The complete BMSC medium was 89% RPMI-1640 (11,875,093, Thermo Fisher Scientific Inc.) + 10% FBS + 1% double antibody. The complete BMSC medium was used as the solvent, and WJ and WJMA microparticles were used as solutes. The leaching solution was prepared according to the existing leaching solution preparation standard ISO 10993–12 (GBT16882.12). BMSCs (mouse20210419-52, Shanghai HonSun Biological Technology Co., Ltd, China) were inoculated in a 96-well cell culture plate with 5×10^3 cells in 100 μl culture medium per well. The outer ring space of the cell culture plate was filled with PBS. After incubating at 37 °C and 5% CO_2 for 24 h, the culture medium was changed to the leaching solution and then changed every 2 days. After culturing with the leaching solution for 3, 5, and 7 days, the CCK-8 reagent was used to measure the OD at 450 nm using an enzyme-labeling instrument. After rehydrating with BMSC complete culture medium for 4 h, the membranes were placed in a 48-well cell culture plate and inoculated with a 100 μl concentrated solution of BMSCs at a cell density of 10^4/100 μl. After incubation at 37 °C and 5% CO_2 for 4 h, the BMSC complete culture medium was used to replenish each well to 500 μl, and the outer ring space of the 48-well cell culture plate was filled with PBS. The cell medium was changed every 2 days. After 3, 5, and 7 days of culture, 50 μl of CCK-8 solution was added to each well. After incubation for 2 h in a cell culture box without light, the medium was transferred to a 96-well plate, and the OD value at 450 nm was measured with the enzyme-labeling instrument. The proliferation rate of cells on the diaphragm were calculated. The result of the cell proliferation experiment was represented by the relative growth rate = (experimental group − blank group)/(G group − blank group).

A cell viability staining kit (C2015C-3, Beyotime Biotechnology Co., Ltd, Shanghai) was used for cell viability staining. After discarding the medium and gently cleaning with PBS twice, 150 μl calcein AM/PI working solution was added to each well for 30 min incubation in dark. The staining was then observed under a fluorescence microscope.

2.3.3. SEM observation of BMSCs on the membranes

After culture of BMSCs on the membranes for 3 days, the membranes were gently washed with PBS twice, fixed with Gluta electron microscope fixative solution (P1126, Beijing Solarbio Science & Technology Co., Ltd) for 6 h, freeze dried, and stored at 4 °C. The membranes were then sprayed with gold, and SEM was used to observe the attached cells.

2.3.4. Cell migration

The migration of BMSCs to the membranes was measured by a Transwell-migration assay. After rehydrating for 4 h, the membranes

were trimmed to a suitable size and placed in the lower chamber of a Transwell plate (REF3422, Costar Co., Ltd). Then, 4×10^4 BMSCs in 200 μl BMSC complete culture medium suspension were seeded in the upper chamber, and 500 μl BMSC complete culture medium was added to the lower chamber. After incubation at 37 °C and 5% CO_2 for 24 h, the culture medium was discarded, and the upper chamber was gently washed with PBS three times. Then, the Transwell chamber was fixed in 4% paraformaldehyde (C190427, Beijing Yangguangyingrui Biology Science and Technology Co., Ltd, Beijing) for 20 min and stained with 0.1% crystal violet (G1064, Beijing Solarbio Science & Technology Co., Ltd) for 20 min in dark. After wiping off the cells that did not penetrate the filter with cotton swabs, cells that migrated to the lower surface of the filter were examined with a microscope (Axiolab 5, Beijing Precise Instrument Co., Ltd, Beijing). The cell number was semi-quantified by detecting the OD value at 450 nm after destaining in 33% acetic acid (A116166, Shanghai Aladdin Biochemical Technology Co., Ltd).

2.3.5. Osteogenic differentiation

After culture of BMSCs on the membranes with osteogenic induction medium (89% RPMI-1640 + 10% FBS + 1% double antibody + 10 mmol/L β-sodium glycerophosphate + 0.05 mmol/L vitamin C + 100 mmol/L dexamethasone) for 7 and 14 days, BMSCs in each group were stained with an alkaline phosphatase (ALP) staining kit (P0321S, Beyotime Biotechnology Co., Ltd) and photographed, and the activity of ALP was measured using a p-nitro-phenylphosphate liquid system. Briefly, after washing with PBS, the membranes were repeatedly blown with RIPA lysis buffer (P0013B, Beyotime Biotechnology Co., Ltd), and the supernatant was collected and reacted with the ALP activity detection kit (C3206, Beyotime Biotechnology Co., Ltd). The OD value was detected at 405 nm to determine the content of p-nitrophenol. Additionally, the intracellular protein concentration was measured by BCA method using the cell lysate. Finally, the relative ALP activity was calculated.

Real-time polymerase chain reaction (RT-PCR) was used to detect the expression of osteoblast-related genes by BMSCs at different time points. The total RNA was collected by Trizol (REF15596018, Life Technology Co., Ltd, USA), which was reversely transcribed into complementary DNA (cDNA) using an RNA-to-cDNA premix kit (RR047A, Takara Bio Inc., China). The gene expressions of runt-related transcription factor 2 (RUNX-2), osteocalcin (OCN), osteopontin (OPN), and collagen type I (COL-I) were quantified using Rotor-gene Q with SYBR Premix Ex Taq II (RR820A, Takara Bio Inc.). The data were analyzed by the $2^{-\Delta\Delta CT}$ method. All gene expression data were normalized to GAPDH (B661304-0001, Sangon Biotech Co., Ltd, Beijing) expression data and expressed as a fold ratio of the blank control. The primers (Sangon Biotech Co., Ltd) used are listed in Table 1.

2.4. In vivo studies

The animal experiments were approved by the Institutional Animal Care and Use Committee (ZJU20160455) and they followed the ARRIVE

Table 1
Primers used for qRT-PCR assay.

Gene	Sequence (5′-3′)
GAPDH-hF	TGGTGAAGCAGGCATCTGAG
GAPDH-hR	TGAAGTCGCAGGAGACAACC
Runx-2-hF	CCTCAGTGATTTAGGGCGCA
Runx-2-hR	ACTTGGTGCAGAGTTCAGGG
OCN-hF	CTGCGCTCTGTCTCTCTGAC
OCN-hR	GCCGGAGTCTGTTCACTACC
OPN-hF	CTTTACAGCCTGCACCCAGA
OPN-hR	TTCTGTGGCGCAAGGAGATT
COL-I-hF	TTCGTGACCGTGACCTTGAG
COL-I-hR	TCTCCGCTCTTCCAGTCAGA

Guidelines. Adult Sprague–Dawley rats (male, 250–300 g, SPF Biotechnology Co., Ltd. Beijing) were randomly divided into five groups (six rats in each group) to receive the G, G-E, G-W, and G-E-W membranes, or serve as a blank control. Intraperitoneal injection of 3% pentobarbital sodium was used for anesthesia. After skin preparation on top of the skull, the unilateral skull was completely exposed, and a round full-thickness defect with a diameter of 5 mm was formed by a drill bit with an outer diameter of 5.5 mm [20,45–48]. Membranes with 4 h of rehydration were used to cover the defect area and then sutured. For the Control group, after the defect was formed, the wound was sutured directly. Postoperative wound infection and positive allergic reaction were checked regularly. Three rats in each group were randomly selected and killed with CO_2 at 4- or 8-weeks post operation. The skull specimens were obtained and fixed with 4% polyformaldehyde overnight.

2.4.1. General observation and micro-CT

The specimens were photographed with a digital camera to grossly observe the bone repair. Micro-CT (GE e Xplore Locu Co., Ltd, USA) was used to scan the specimens with a scanning resolution of 48 μm, a rotation angle of 360°, and a voltage of 80 kV. The data were then reconstructed using the bundled software (GEHC MicroView). The region of interest was set as the skull defect size (a cylinder with a height of 0.8 mm and a diameter of 5.5 mm), and the relative bone volume (BV/TV), trabecular thickness (Tb·Th), trabecular number (Tb·N), trabecular separation (Tb.Sp), bone mineral content (BMC), and bone mineral density (BMD) were quantitatively analyzed.

2.4.2. Histological analysis

The fixed specimens were decalcified with ethylene diamine tetra-acetic acid (EDTA, N20200612, Beijing Yilichemicals Co., Ltd, Beijing) at room temperature for 4 weeks, dehydrated with an automatic dehydrator (ASP300S, Leica Biosystems Co., Ltd, Shanghai), embedded in paraffin, and cut into 5-μm thick slices. The sections were then treated with hematoxylin and eosin (H&E) staining and Masson trichrome staining (G1340, Beijing Solarbio Science & Technology Co., Ltd). The images were obtained with a microscope (BX50F-3, OLYMPUS OPTICAL Co., Ltd, Japan).

2.4.3. Histological analysis of important organs

For the 8-week healing group, the heart, liver, spleen, lung, and kidney were harvested, fixed with 4% paraformaldehyde overnight, dehydrated, embedded in paraffin, and cut into 5-μm slices. H&E staining was performed and images were obtained.

2.5. Statistical analysis

The data were expressed as mean ± standard deviation. The data were analyzed by SPSS Statistics 26 with a two-sided *t*-test or one-way analysis of variance followed by a SNK-*q* test. $P < 0.05$ was considered to have statistical difference, and $p < 0.01$ was considered to have significant statistical difference. All pictures were drawn by Origin 2018 and processed by Adobe Photoshop 2020 and Adobe Illustrator 2020.
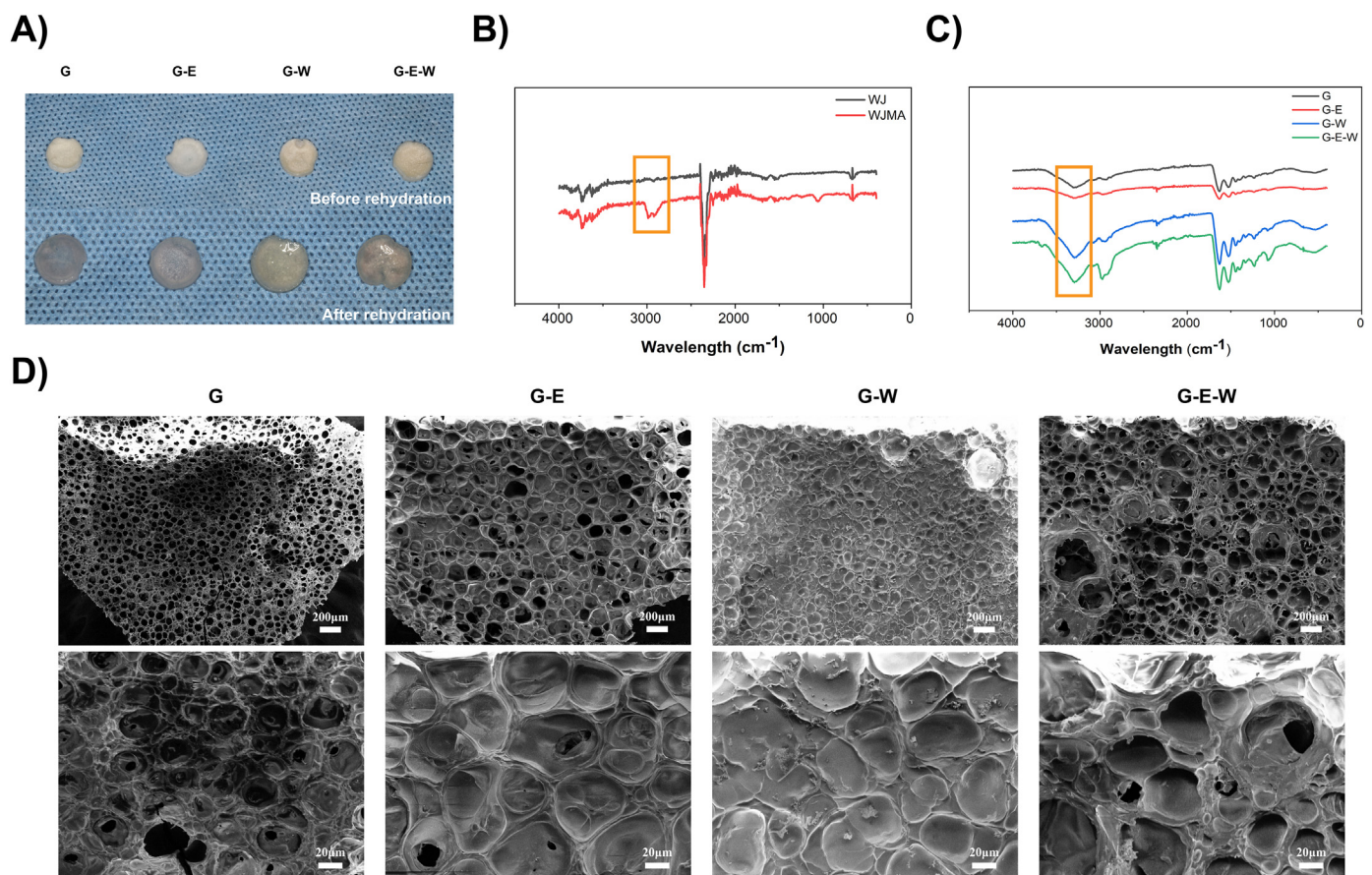

Fig. 2. Characterization of the G-E-W artificial periosteum. A) The morphology of the materials after freeze-drying and rehydration. B) Difference in infrared spectra between WJ and WJMA as indicated by the grafting and the formation of new bonds. C) Difference in infrared spectra between G, G-E, G-W and G-E-W artificial membranes indicating that there was a new chemical bond between WJMA and G in the G-W and G-E-W artificial membranes. D) SEM observation of the G, G-E, G-W and G-E-W artificial membranes. G, GelMA membrane; G-E, GelMA-E7membrane; G-W, GelMA-WJMA membrane; G-E-W, GelMA-E7-WJMA membrane; WJ, wharton's jelly; WJMA, WJ after methacrylic anhydride treatment.

3. Results and discussion

3.1. Preparation and characterization of the membranes

3.1.1. General view of the artificial periosteum membranes

Intact membranes with a thickness of 1 mm were successfully fabricated by photo-crosslinking of GelMA with WJMA with or without E7. Slight differences in gross color were observed. The freeze-dried membranes without WJMA were milky white, while the membranes with WJMA were pale yellow. The freeze-dried membranes had no viscosity, while those after rehydration were gel-like with a certain viscosity (Fig. 2A). There were only short peptides and GelMA hydrogel in G and G-E, and the proteins and GelMA themselves were colorless and tasteless, so they were transparent. However, after WJMA was added, there were more microparticles in the membranes, resulting in the opaque, pale-yellow color.

3.1.2. Fourier transform infrared spectrometer results

The FTIR results show the WJMA had obvious peak differences at approximately 3000 cm^{-1} relative to WJ (Fig. 2B). The amide B band was approximately 3078 cm^{-1} [41], confirming MA was successfully cross-linked with WJ by forming an amide bond. Compared with G, the G-W and G-E-W groups showed an obvious peak pattern change at approximately 3300 cm^{-1}, and the peak decline rate became slow, while G-E showed no obvious difference (Fig. 2C). The amide A band was located at approximately 3360 cm^{-1} [41], and the peak pattern change proved that there was chemical bond formation between GelMA and WJMA [42,49]. Scholars have introduced the 'Bicomponent polymer network (BCN)', a network system comprising two chemically different polymer sequences that are covalently bound by concentrated chemical bonds and combine different functional biomaterial aggregates into a stable network structure to realize complementarity of the components [50,51]. The FTIR results showed that the combination of GelMA and WJMA, though physically mixed, can also form amide bonds by photo-crosslinking. This special structure can be distinguished from interpenetrating networks containing two or more independent networks, and it could not be separated without breaking covalent bonds [50]. The mechanical properties test proved that GelMA and WJMA formed a stable connection.

3.1.3. Microscopic structural observation

The SEM observations show that the membranes had three-dimensional microporous structures. The pores in G and G-E were relatively uniform in size and G-E had a larger micropore diameter. For G-W and G-E-W, the pore size was uneven, and a scattered distribution of the WJMA microparticles was observed (Fig. 2D). The porosity and interconnectivity of materials are very important for the effective diffusion of nutrients and gases that create a protected and supportive environment for cell inoculation. The porous nature of the four membranes contributed to the metabolism of cells regenerated in the membranes and met the metabolic needs of tissues [52]. In the WJMA group, the pore sizes of the G-W and G-E-W groups were not uniform; however, the basic pore structure remained unchanged, which was still beneficial to cell adhesion, growth, and metabolism.

3.1.4. Water contact angle results

Generally, the freeze-dried membranes showed relatively large water contact angles and were considered hydrophobic. G had a water contact angle of 70.29°, and the addition of E7 peptide (G-E) increased the water contact angle to 85.50°. The addition of WJMA (G-W and G-E-W) significantly increased the water contact angles to 91.42° and 95.80°, respectively (Fig. 3A and B). The measurements allowed for the analysis of the contact angle of a liquid on the solid surface and the evaluation of the hydrophilicity, hydrophobicity, and wettability of the material surface, all of which affect the inoculation, migration, adhesion, and growth of cells. In this experiment, the addition of WJMA increased the contact angle of hydrogel before rehydration; however, the change was small and within an acceptable range. After adding WJMA, the increase in the
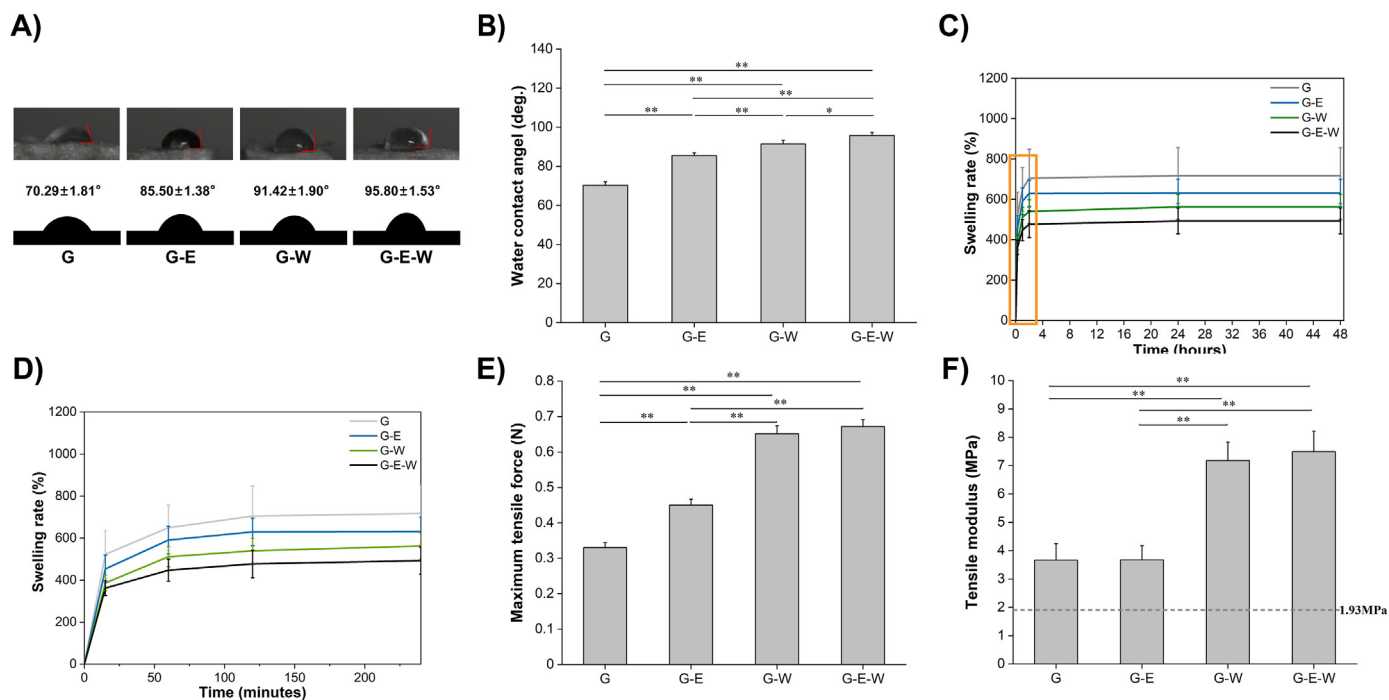

Fig. 3. Characterization of the G-E-W artificial periosteum. A, B) Morphological changes and statistical analysis of the water contact angle. C, D) Swelling ratio of the G, G-E, G-W and G-E-W artificial membranes. E, F) Maximum load value and tensile modulus analysis of the artificial periosteum after rehydration. Data were expressed as mean ± SD (*$p < 0.05$, **$p < 0.01$). G, GelMA membrane; G-E, GelMA-E7membrane; G-W, GelMA-WJMA membrane; G-E-W, GelMA-E7-WJMA membrane.

water contact angle might be attributed to the addition of WJMA micropowders, which changed the pore of the freeze-dried hydrogel, resulting in a decrease in its water absorption performance.

3.1.5. Swelling results

For all of the time points in this study, the swelling rate of the membranes followed the trend of G-E-W < G-W < G-E < G. Generally, the membranes showed similar swelling profiles that reached water absorption saturation quickly after 2 h of immersion (Fig. 3C and D). After 2 h of swelling, the swelling rate was 492.97%, 562.68%, 717.58%, and 631.75% the original mass for G-E-W, G-W, G-E, and G, respectively. Hydrogels absorb and retain a large amount of water, which can affect the solute diffusion, surface properties, and mechanical properties. The swelling ratio indicates the water absorption of the material, which can reflect the absorption of nutrient medium. This property is extremely important for the activity, growth, and differentiation of cells [53]. The GelMA used in this experiment was uniform; as a result, the biggest factor affecting the swelling rate of the experimental membrane was not the methylation degree, but the type and content of the added material. After adding WJMA, the swelling rate of the material decreased because the barrier to water molecules entering the hydrogel increased, resulting in the water entry and swelling rate decreasing.

3.1.6. Mechanical testing results

According to the tensile test results, the addition of the E7 peptide slightly increased the tensile strength. With the addition of the WJMA microparticles, the tensile strength of G-W and G-E-W was markedly enhanced relative to G and G-E. The elastic modulus of natural periosteum was generally 0.92–1.93 MPa [54], while the tensile modulus of the four types of membranes were all greater than that of natural periosteum, and the tensile modulus of the G-W and G-E-W groups were improved (Fig. 3E and F). Although the stability of the physical embedding method was poor, after adding WJMA micropowders, the structure was stable after photo-crosslinking by photo-taking groups. The mechanical strength of grafted WJ and GelMA was greater than that of the G and G-E groups. The chemical bond formed by WJMA and GelMA enhanced the mechanical properties of the membrane, which was more conducive to maintaining the stability of the membrane while resisting the movement of bone defects or fractures.

3.1.7. Degradation and pH changes

After 4 h of swelling in PBS, the membranes were placed in simulated body fluid to assess their degradation. Over time, the remaining mass of the membranes decreased (Fig. 4A). The durations needed for complete degradation of the G, G-E, G-W and G-E-W membranes were nearly the same at approximately 36 days. Between Day 4 and Day 24, the degradation percentage followed the trend of G-E-W < G-W < G-E < G (Fig. 4B). After an ideal biomaterial is implanted in the host defect area, the degradation time of the material should match the tissue regeneration speed in the host defect area. If the degradation rate of the material is too fast, it is not conducive to the colonization and regeneration of cells. If the degradation rate is too slow, it would hinder the new tissue from creeping substitution to the defect center. Because of the barrier of WJMA micropowders, it was difficult for water to enter the membranes of the G-W and G-E-W membranes; as a result, the swelling ratios of the G-W and G-E-W membranes were relatively small. WJMA can also crosslink with GelMA, which improves the cross-linking degree of the materials such that it was more difficult for water to enter the G-W and G-E-W membranes. However, crosslinking can also reduce the corrosion effect of liquid on the membranes; as a result, the G-W and G-E-W membranes had slower degradation rates than the G and G-E membranes.

The changing profiles of the pH of the simulated body fluid during membrane degradation with time were nearly the same for all membranes. The pH values of the simulated body fluid first decreased from
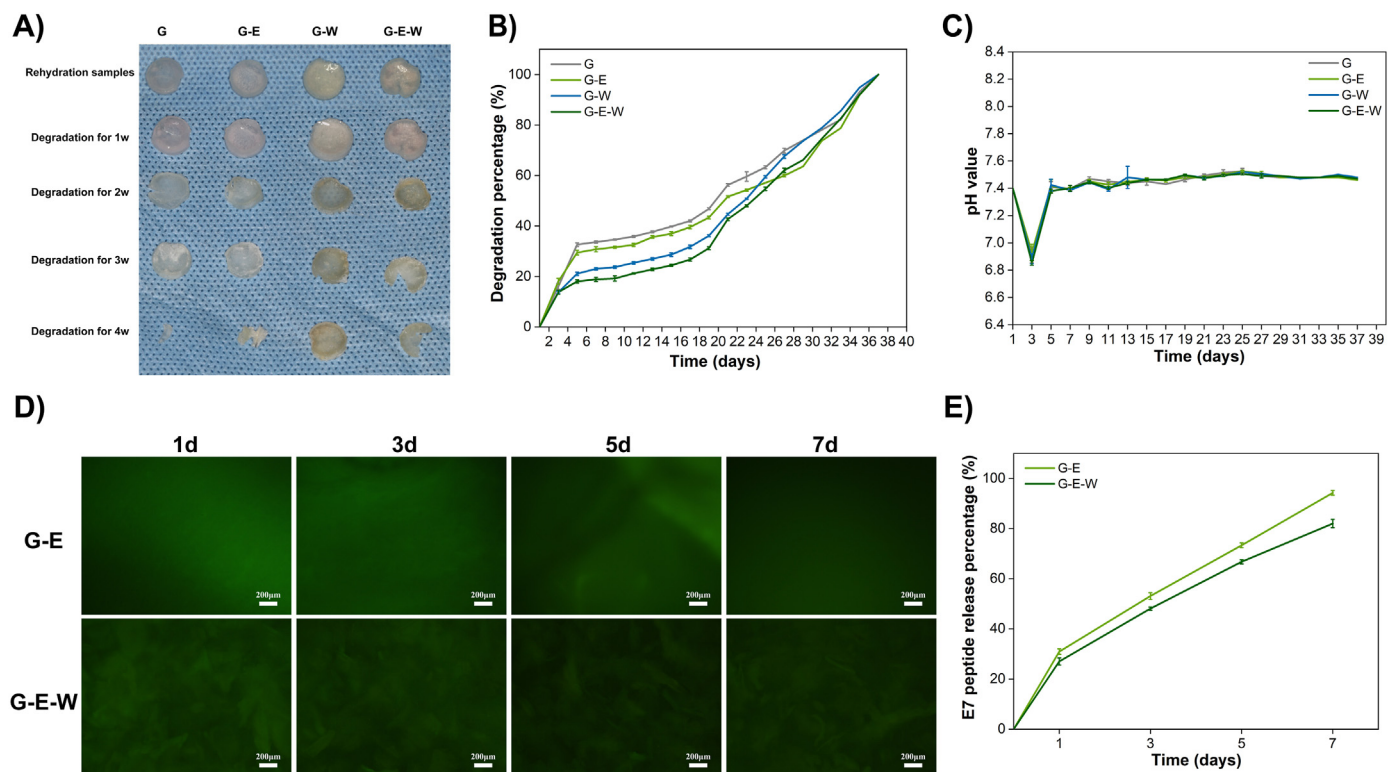

Fig. 4. Characterization of the G-E-W artificial periosteum. A) Changes in the morphology of G, G-E, G-W and G-E-W artificial membranes during degradation. B) Degradation rates of the G, G-E, G-W and G-E-W artificial membranes. C) Changes in pH during degradation of the G, G-E, G-W and G-E-W artificial membranes. D, E) Fluorescent E7 peptide was used to observe the retention time and release percentage of E7 peptide in the G-E and G-E-W membranes. Data were expressed as mean ± SD (*$p < 0.05$, **$p < 0.01$). G, GelMA membrane; G-E, GelMA-E7membrane; G-W, GelMA-WJMA membrane; G-E-W, GelMA-E7-WJMA membrane.

7.4 to 6.8 from Day 0 to Day 2, then recovered to approximately 7.4 at Day 4, and remained relatively stable (Fig. 4C). The change in pH of the artificial body fluid caused by the degradation process of the material in the early stage was the acid release phenomenon after GelMA rehydration and it was within an acceptable range [41], which proved that the selection of the material and the degradation process were beneficial to cells. The mechanical properties and water absorption of the matrix affect the behavior of MSCs [55], and it was reported that with an increase in GelMA concentration, its tensile modulus and compressive modulus would also increase [56,57]. Concurrently, the swelling characteristics of the hydrogel would also affect the surface characteristics, diffusion rate, and mechanical properties of the material [57]. Therefore, finding the appropriate concentration and the best ratio with other ingredients increase the physical and chemical properties of the membrane, as well as improve its biocompatibility.

3.1.8. Stability of E7 peptide in the membranes

G-E and G-E-W prepared with fluorescent E7 peptide still showed a fluorescence signal after incubation in the simulated body fluid in dark for as long as 7 days, indicating the long lasting existence of E7 peptide in the membranes for at least 7 days (Fig. 4D). Quantitative experiments also reached the same conclusion, and the release of fluorescent E7 peptide in G-E-W was slower than that in G-E (Fig. 4E). The decrease of the fluorescence intensity with time was ascribed to the controlled release of E7 peptide accompanied with the membrane degradation.

Although the fluorescent E7 peptide in the membranes gradually dissipated with time, the persistence of fluorescence confirmed the existence of E7 peptide in the membrane suggesting E7 could recruit and anchor BMSCs. Because of the WJMA micropowders in the G-E-W group, E7 peptide had more adhesion sites, resulting in the fluorescent E7 peptide having flake- and dot-like shapes. Because of the increase in the adhesion sites, the dissipation and loss rate of the E7 peptide in the G-E-W group was less than that in the G-E group, which proved that WJMA micropowders in the G-E-W group could prolong the retention time of E7 peptide, making the migration and differentiation of endogenous stem cells or progenitor cells more lasting, and further improve the osteogenesis rate of the materials. The stability and structure of the E7 peptide will not be damaged by the ultraviolet light used during photocrosslinking [58], and the irradiation sterilization will not affect the E7 peptide in WJMA that is added during material treatment [41]. Therefore, the E7 peptide stored in the membrane that exert the most stable and maximum benefit was evaluated in a follow-up experiment.

3.2. In vitro cell experiment

3.2.1. Biocompatibility of the artificial periosteum membranes

To evaluate whether the membranes have cytotoxicity, L929 cells were cultured in the leaching solution of the membranes for 1, 3, and 5 days. The CCK-8 measurement showed that the relative growth rate of the four membranes at all time points was greater than 0.75 (Fig. 5A).
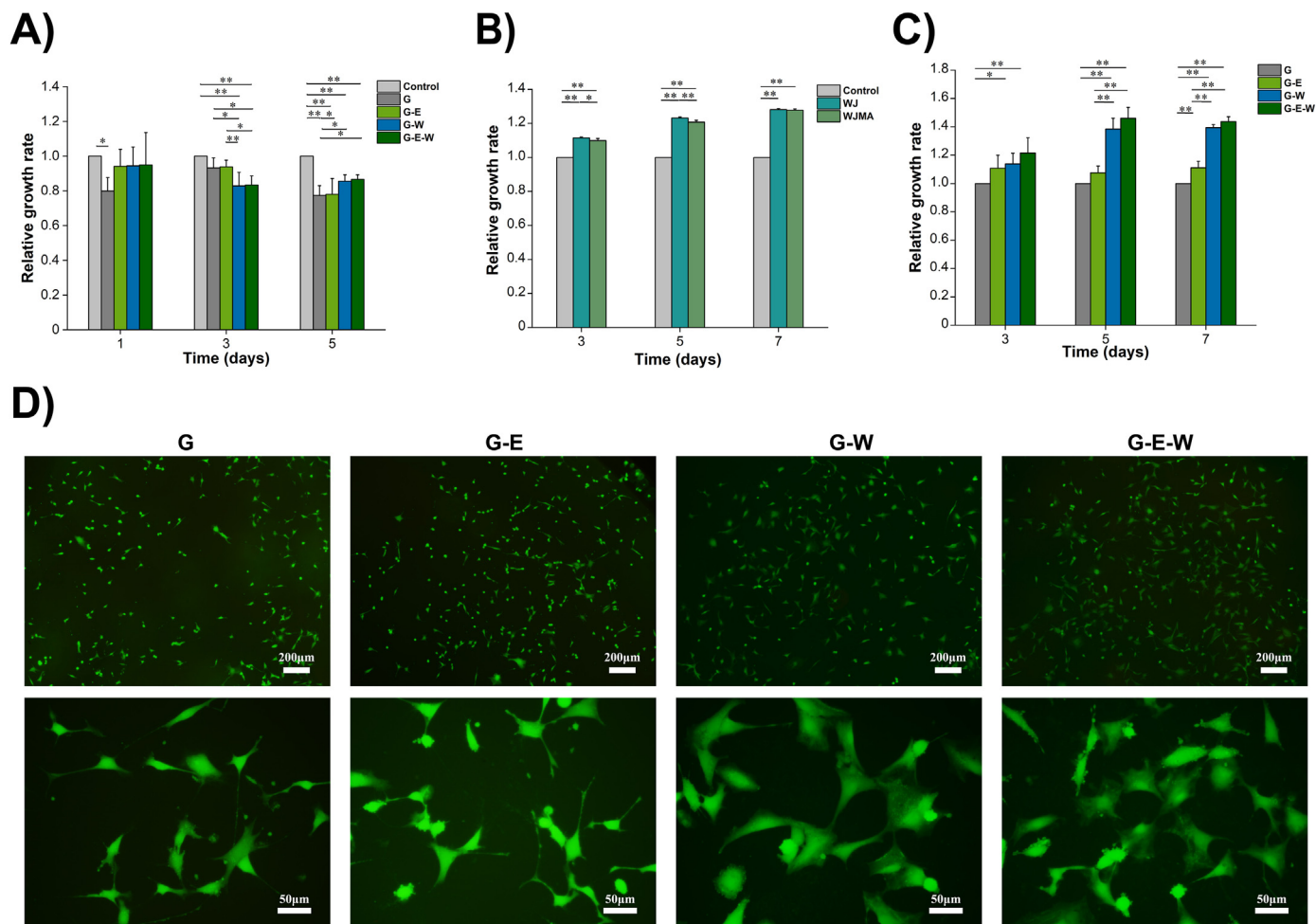

Fig. 5. Vitality of cells growing on the membranes. A) The membranes were used to prepare a leaching solution for the cytotoxicity test. B) Proliferation rate of BMSCs in the WJ and WJMA leaching solution. C) Proliferation rate of BMSCs on the membranes for 3, 5, and 7 days. D) Live/Dead staining of BMSCs on membranes for 3 days; green fluorescent cells were alive and red fluorescent cells were dead. Data were expressed as mean ± SD (*$p < 0.05$, **$p < 0.01$). G, GelMA membrane; G-E, GelMA-E7membrane; G-W, GelMA-WJMA membrane; G-E-W, GelMA-E7-WJMA membrane.

According to the standard of toxicity grading method of the United States Pharmacopoeia, the four membranes were categorized as cytotoxicity grade I. Although the cytotoxicity test confirmed that the material could be used for the next cell experiment, the cytotoxicity still did not meet the requirements of grade 0. The low cytotoxicity may be attributed to the GelMA, which although it still has slight toxicity, met the requirements of biocompatibility. Additionally, WJ was treated with MA, which is a slightly toxic product. After grafting and crosslinking, the residual MA might not be removed, resulting in cytotoxicity.

3.2.2. Cell proliferation and viability staining

The biological compatibility of the material can be reflected by the relative growth rate after co-culture with the materials and morphological observation of the cells using Live/Dead staining. The results of BMSCs cultured with the WJ and WJMA leaching solutions showed that the cell proliferation of the WJ containing group was superior to the blank control group at any detection time (Fig. 5B). The proliferation of BMSCs on the membrane surfaces was assessed and the results showed that the cell proliferation among the membranes followed the rank of G-E-W > G-W > G-E > G at all measured time points (Fig. 5C). Compared with the G membranes, the G-E membrane had a slightly promoted cell proliferation; however, the main function of E7 peptide was to recruit and anchor BMSCs. This phenomenon proved that E7 peptide had a chemotactic effect of BMSC recruitment, and also slightly promoted BMSC proliferation [35,59]. Compared with the other membranes, the G-E-W membranes had significant ability to promote cell proliferation, which might be related to the numerous cytokines in WJMA. WJ originally belongs to human umbilical cord tissue, which is an important medium for connecting the mother and fetus. WJ contains few cells and a lot of ECM, and is rich in COL, HA, and proteoglycan. Insulin growth factor, fibroblast growth factor, and transforming growth factor can accumulate in WJ, thus promoting the synthesis of ECM [27]. It has been reported that WJ contains numerous exosomes of α-2-macroglobulin (α2M), and α2M is considered the main component that promotes wound healing [60]. E7 peptide can recruit MSCs in the early stage, and the stimulation of cytokines in WJ can make the recruited MSCs and in situ cells proliferate in large quantities, providing the foundation for later osteogenesis.

As shown in the Live/Dead staining images of BMSCs cultured on membranes for 3 days (Fig. 5D), the cells on the four membranes were all vital with green staining and no dead cells were stained in red, demonstrating the biocompatibility of the membranes. More BMSCs were observed on G-E-W and G-W than G-E and G, consistent with the cell proliferation assay results. Additionally, BMSCs on G-E-W and G-W had significantly larger spreading areas than those on G-E and G.

3.2.3. SEM observation of BMSCs on the membranes

In the process of cell culture, the cell morphology can reflect cell growth to a certain extent. Because of the organic polymer nature, the membranes would melt in the environment of a high thermal electric field after a long time [41], so it was necessary to take a snapshot using SEM. In the four G, G-E, G-W, and G-E-W membranes, the BMSCs fixed on the surface of each membrane were observed, and the shape of BMSCs in each group was normal. In the same field of vision, there were more BMSCs in the membrane with the E7 peptide group (Fig. 6A). Co-culture SEM results showed that MSCs could adhere and grow normally on the membrane materials, and GelMA, E7 peptide, and WJMA had no effect on the morphology of BMSCs, which demonstrates the relationship between the adhesion, growth, and morphological changes of MSCs on the membranes.

3.2.4. Cell migration

E7 peptide can recruit BMSCs in vivo and in vitro, promote BMSC homing to bone defects, and promote BMSCs adhesion and proliferation [59,61]. In this study, the E7 peptide was used for in situ recruitment of MSCs. G-E-W, G-W, and G-E recruited substantial amounts of BMSCs, while G only recruited a few cells (Fig. 6B). Quantitatively, the OD values of the material groups with E7 peptide were greater than those of the G and G-W membranes (Fig. 6C), and there was a significant statistical difference between the membranes with and without with E7 peptide on BMSC migration ($p < 0.01$). The number of cells recruited in G-W may be related to the strong effect of WJ on cell proliferation. The statistical results confirm the high affinity, recruitment, and anchoring effect of E7 peptide on BMSCs. The in vitro culture of MSCs before implantation was also an innovation of this project. In vivo in situ recruitment of stem cells could avoid the tedious process of in vitro seed cell culture and the occurrence of immune-derived diseases.

3.2.5. Osteogenic differentiation

Agathocleous et al. reported that cells will lose their ability to divide after differentiation [62]. Based on the promising results of osteogenesis and mineralization in vitro, BMSCs were used to explore the osteogenesis-inducing ability of membrane materials. ALP is a marker of early osteogenesis mainly responsible for the mineralization of ECM
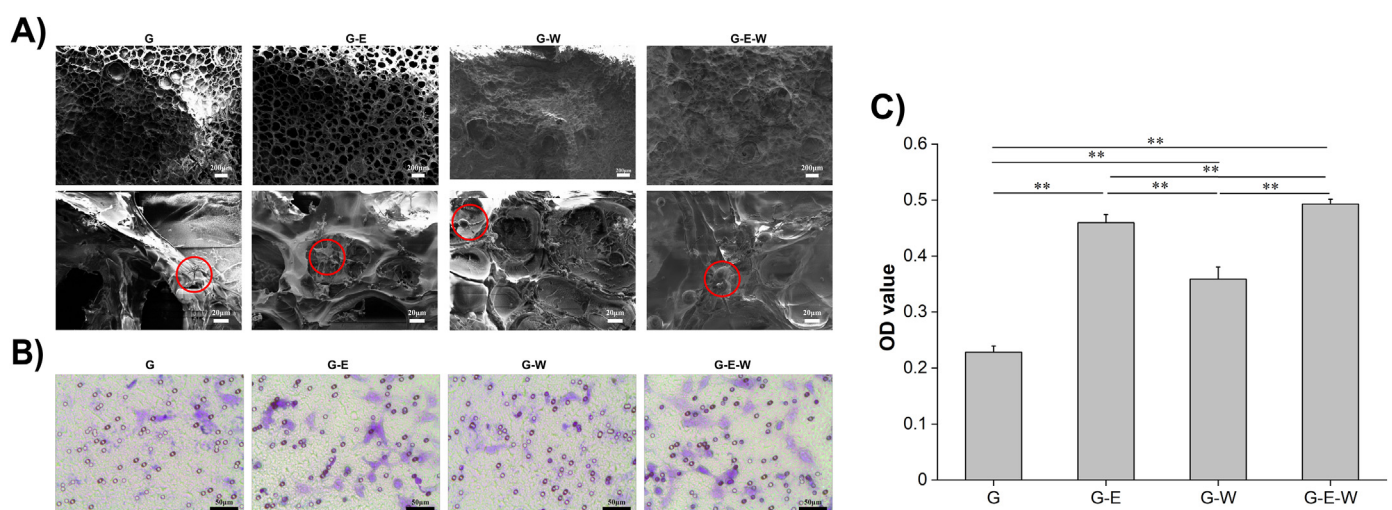

Fig. 6. Vitality of cells growing on the membranes. A) SEM observation of BMSCs growing on the membranes for 3 days. B) A transwell chamber was used to observe the recruitment of BMSCs by the membranes. C) Quantification of the recruitment effect of the membranes on BMSCs. Data were expressed as mean ± SD (*$p < 0.05$, **$p < 0.01$). G, GelMA membrane; G-E, GelMA-E7membrane; G-W, GelMA-WJMA membrane; G-E-W, GelMA-E7-WJMA membrane; OD, optical density.

[63], which is mainly responsible for hydrolyzing organophosphate, increasing the local PO_4^{3-} concentration, accelerating Ca^{2+} deposition, and regulating bone matrix calcification [64]. As a result, ALP is often evaluated to track the osteogenic differentiation of cells. After 7 and 14 days of culture, the ALP expression by BMSCs on different membranes followed the trend of G-E-W > G-W > G-E > G (Fig. 7A and B). The experimental results showed that the expression of ALP was significantly increased in the groups with E7 peptide and WJMA, potentially because the E7 peptide makes more BMSCs anchor and recruit, and the growth factors in WJMA accelerate the proliferation and differentiation of MSCs. Although the increase in ALP expression was not obvious at 7 days, the positive effect of the composite membrane group on ALP expression became more obvious with time. The G-E-W membrane had a positive significance for bone differentiation in the early stage of osteogenesis.

In addition, alizarin red staining can be used to evaluate the formation of mineralized nodules in late osteogenesis [65]. Because the hydrogel membrane and BMSC co-culture system were used for dyeing in this experiment, the alizarin red dye solution replaced the water in the hydrogel in the dyeing stage and it was impossible to take pictures and quantify the nodules.

The gene expression levels of RUNX-2, OCN, OPN, and COL-I by BMSCs cultured on the membranes at 7 and 14 days are shown in Fig. 7C. For the gene marker of early osteogenesis, the expression level of RUNX-2 in the G-W and G-E-W membranes was greater than that in the G group at 7 days ($p < 0.01$), and the expression level of RUNX-2 in the group with E7 peptide and WJMA maintained the trend at 14 days ($p < 0.01$). For the gene markers of late osteogenesis, OCN and OPN, the expression of OCN in the G-E-W membrane was significantly greater than that in the other membranes at 7 days ($p < 0.01$), and the gene expression in the G-W and G-E-W membranes was greater than that in the G group ($p < 0.01$); on 14 days, the OCN expression was more obvious in membranes with WJMA ($p < 0.01$). The expression of OPN gene in the G-E-W membrane was significantly greater than that in the G and G-E membranes at 7 and 14 days ($p < 0.01$), and this trend was maintained with time. At 7 days, the gene expression of COL-I was significantly greater in the membrane with WJMA than without ($p < 0.01$). At 14 days, the trend was down significantly; however, there was still a statistical difference between them ($p < 0.05$). As shown in the RT-PCR results, the expression of RUNX-2, an early osteogenic gene marker, and OCN, OPN, late osteogenic gene markers changed at different time periods; however, they did not affect the final osteogenic process that was related to the unique recruitment and anchoring effect of the E7 peptide on stem cells and the abundant cytokines in WJMA. Both E7 peptide and WJMA significantly promote cell proliferation, and the expression of osteogenic genes in the early stage may be related to the cell growth state and high cell density, while the expression of osteogenic genes in the late stage may be related to the growth factors in WJMA and the natural reaction of osteogenesis. Specifically, with the addition of E7 peptide and WJMA, the osteogenic ability was more prominent, which further enriched the diversity in the selection of bone tissue engineering materials. Additionally, drugs or bioactive factors coated with hydrogel can promote bone regeneration; however, the cross-linked structure of the hydrogel can support cell infiltration and migration [6,66]. Therefore, the combination of GelMA hydrogel with E7 peptide and WJMA in this experiment can support and
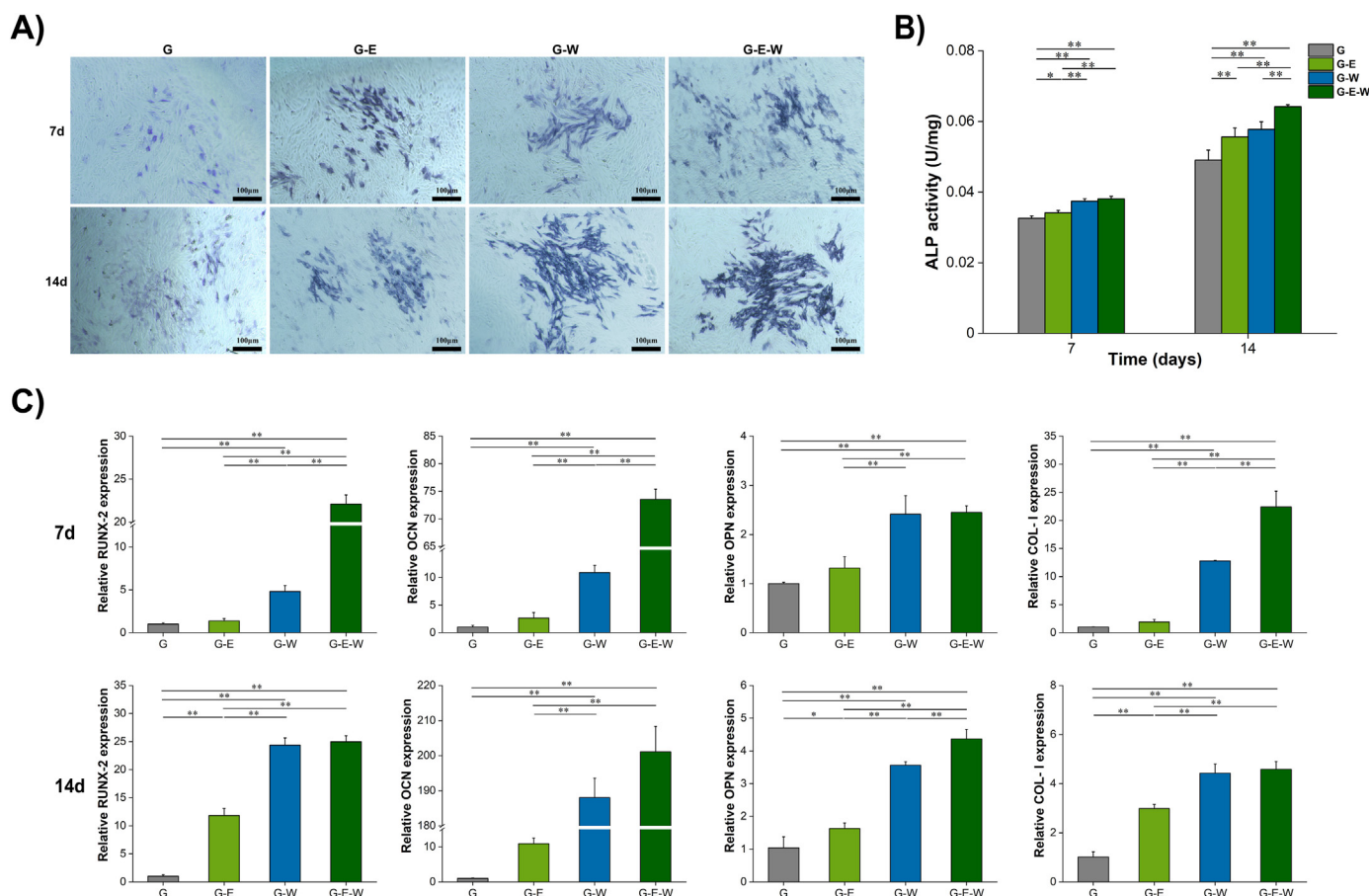

Fig. 7. Osteogenic expression of cells growing on the membranes. A, B) The ALP of BMSCs growing on the membranes for 7 and 14 days to track the early osteogenic differentiation of cells. C) The expression of RUNX-2, OCN, OPN, and COL-I genes of BMSCs growing on the membranes for 7 and 14 days. Data were expressed as mean ± SD (*$p < 0.05$, **$p < 0.01$). ALP, alkaline phosphatase; G, GelMA membrane; G-E, GelMA-E7membrane; G-W, GelMA-WJMA membrane; G-E-W, GelMA-E7-WJMA membrane.

promote the bone repair process of bone defects from many aspects, angles, and dimensions.

3.3. In vivo cell experiment

3.3.1. General observation of rat skull defect samples

After the materials were implanted in the rat skull defect (Fig. 8A), the models of the skull defect were taken at 4 and 8 weeks. During the sampling process, some 4-week sampling groups showed that there were residual membrane samples in the bone defect, and the residual membrane samples were incomplete; however, none were found in the 8-week sampling group. After the rat skull defect models were taken, the specimens were ruddy in color, without obvious abnormality or osteophytes (Fig. 8B). At 4 and 8 weeks, the healing of the defect in the G-E-W group was better than that in the G, G-E, G-W, and NC groups, while the healing of the G-E and G-W groups was better than that of the NC and G groups. Additionally, there was almost no obvious difference in the degree of defect healing between the NC and G groups at 4 and 8 weeks. Combining the in vitro degradation experiment with the observations of the sample residue at 4 weeks, the degradation process of samples in vivo might be slightly faster than that in vitro. Compared with the NC and G groups, the G-E-W group had the best healing of the defect model, followed by the G-E group and G-W group. After adding E7 peptide or WJMA, the osteogenic effect of the bone defect was enhanced, and the combination of E7 peptide and WJMA improves the osteogenic effect.

3.3.2. Micro-CT scanning and reconstruction

Micro-CT scanning of bone defect models can reflect the location and area of new bone formation in the defect more clearly and intuitively (Fig. 8C). At 4 weeks, there was only a small amount of new bone in the NC group, a small amount of bone regeneration around the defect in the G group, obvious bone regeneration in the G-E and G-W groups, and

nearly half of the bone regeneration in the G-E-W group was achieved. At 8 weeks, although there was new bone formation in the NC and G groups, there was still a large area defect; however, in the G-E and G-W groups, the formation of new bone increased markedly, and only a small area of bone defect remained, while in the G-E-W group, a large area of new bone was found at the bone defect that covered the bone defect.

Reconstructing the specimen by micro-CT can more scientifically reflect the repair of bone regeneration in the defect. The above results were quantified by BV/TV; the G-E-W membrane played a significant role in promoting osteogenesis compared with the other membranes ($p < 0.01$), and the Tb·Th and Tb·N results were similar to BV/TV (Fig. 8D). Additionally, the quantitative results of Tb. Sp showed that G-E-W significantly reduced the trabecular dispersion of new bone at 4 and 8 weeks ($p < 0.01$) (Fig. 8D). The quantitative results of BMC and BMD were similar to the NC and G groups; G-E, G-W and G-E-W groups with E7 peptide or WJMA significantly improved the mineral content of the bone tissue ($p < 0.01$) (Fig. 8D). Because E7 peptide and WJMA existed in the G-E-W group at the same time, the interaction between the components and cells promoted the bone repair ability. Compared with the G-E and G-W groups, E7 peptide and WJMA in the G-E-W group promoted osteogenesis more. The BV/TV value of the G-E-W group was significantly greater than that of the other groups, which indicated that the G-E-W membrane can promote the formation of more bone tissue per unit volume. At the same time, the values of Tb·Th and Tb·N in the G-E-W group were also better than those in other groups, indicating that the G-E-W membrane material promotes osteogenesis and the stability of new bone. The significant decrease in the Tb. Sp value in the G-E-W group could indicate that the number of trabeculae in the unit area increases, which is another example of the excellent osteogenesis quality. Both BMC and BMD are related indexes of bone minerals, and their values for the G-E-W group were greater than those in other groups, which proved that the G-E-W membrane promoted bone formation and bone mineralization.
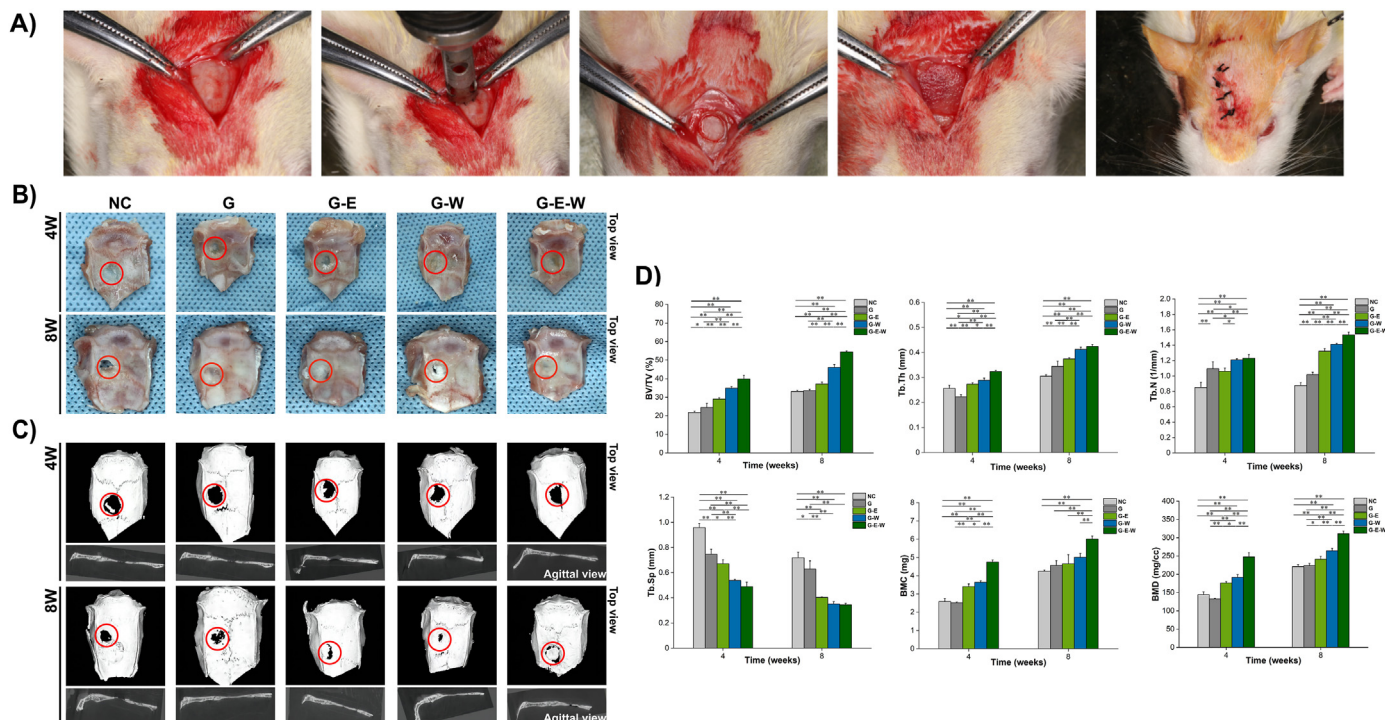

Fig. 8. Macroscopic and micro-CT observation of bone defect repair using the G, G-E, G-W and G-E-W artificial membranes at 4 and 8 weeks. A) Rat skull defect modeling and artificial periosteum implantation. B) Macroscopic observation of the bone defect repair. C) Micro-CT reconstructions of the bone defect repair in the G, G-E, G-W and G-E-W groups. D) Quantification of Micro-CT indicators: bone volume/total volume (BV/TV), trabecular thickness (Tb·Th), trabecular number (Tb·N), trabecular separation (Tb.Sp), bone mineral content (BMC), and bone mineral density (BMD). Data were expressed as mean ± SD (*$p < 0.05$, **$p < 0.01$). G, GelMA membrane; G-E, GelMA-E7membrane; G-W, GelMA-WJMA membrane; G-E-W, GelMA-E7-WJMA membrane; NC, negative control.

3.3.3. Histological analysis of the rat skull defect samples

All rats resumed normal activities within 6 h of operation, and no obvious infection, inflammation, or swelling of the skin in the operation area was observed 8 weeks after the operation. The repaired skull defect was cut to a 5-μm thickness and stained with H&E and Masson. As shown in the histological pictures, nearly all of the samples showed different degrees of new bone tissue formation, and bone marrow cavities of different sizes were formed, especially in the 8-week samples. The thickness of the new bone in all of the 8-week samples was markedly better than that in the 4-week samples. After 4 weeks, new bone tissue with different thickness was observed in all specimens, among which the G-E-W membrane was the best, followed by the G-W membrane, and the G-E membrane, which were superior to the NC and G groups. The same trend was observed at 8 weeks. Additionally, new periosteal tissue was observed with H&E staining to cover the new bone at 4 and 8 weeks, and there was no inflammatory cell infiltration in the histology (Fig. 9A). Masson staining was used to evaluate the formation of COL-I in vivo. In general, the newly generated collagen tissue is colored blue or green, while the mature bone and other substances appear red. After implantation of the membrane, compared with the NC and G groups, the expression of COL-I, the number of bone trabeculae, and the number of mature bone marrow cavities in the G-E-W group were greater (Fig. 9B). The histological results further proved the efficacy of the G-E-W membrane as an artificial periosteum. Imaging and histological analysis showed the G-E-W membrane played the most active role in promoting the quantity and quality of osteogenesis and mineralization. E7 peptide and WJMA in the membrane play a role in osteogenesis and differentiation, respectively; however, their synergistic effect promoting bone formation and differentiation was more obvious, thus highlighting the application potential of the G-E-W membrane.

3.3.4. Histological analysis of important organs

Important organ histology can be used to observe the effect of material metabolism on the body after implantation. Regarding the histological sections of heart, liver, spleen, lung, and kidney tissue at 8 weeks, compared with the NC group, the visceral manifestations of the G, G-E, G-W, and G-E-W membranes were all normal, and there was no obvious change in tissue structure or morphology (Fig. 10).

3.4. Osteogenesis and periosteum

3.4.1. Osteogenesis and BMSCs

Fractures and bone defects are the most common orthopedic diseases in modern society, with a high incidence and that broadly affects the population. How to promote bone repair efficiently and quickly is a problem that must be solved in orthopedic research. The number of MSCs at the fracture site is positively correlated with callus volume and osteogenic ability at the fracture site; however, it negatively correlates with the fracture healing time [67]. The homing characteristics of MSCs can make the bone injury area recruit more MSCs from the surrounding tissue or circulation, thus promoting bone healing and bone regeneration. Although BMSC migration has great potential in the treatment of bone defects, the mechanism controlling MSC migration and signal transduction has not been thoroughly studied. The periosteum is a membrane structure covering the whole bone surface that plays an important role in the bone formation and injury repair. The transplantation of periosteum is also limited by problems of applicability, infectivity, and immune rejection. Imitating the structure and function of the natural periosteum is a new method to expedite the healing of large bone defects, and the use of periosteum with an osteogenic effect can also expedite the osteogenic efficiency of bone grafts with large bone defects.

Bone mineralization is a two-way process. In the first stage, a series of reactions are aimed at realizing the interaction between Ca^{2+}, PO_4^-, and other internal enrichment molecules. The second stage is the proliferation of extracellular hydroxyapatite crystals after the rupture of the basic vesicle membrane and the prefabricated hydroxyapatite crystals exposed to extracellular fluid [68–70]. The proliferation rate of mineral crystals after the second stage strongly depends on the extracellular conditions. Calcium deposition on the 3D network can be changed by changing the indexes of the 3D scaffolds.

3.4.2. Periosteum and selection of periosteum materials

A complex preparation process and multi-material components are burdens for preparing membranes. It is also a great advantage to simplify the preparation process and achieve ideal osteogenic repair effect. In the preparation of the G-E-W periosteum, E7 peptide that can anchor BMSCs is selected as the material to achieve in situ recruitment of endogenous stem cells, thus optimizing the cell source in the process of experiment and repair. Additionally, we only use WJ with low immunogenicity, and no reagents were used in the acellular process. The easier operation enhances the feasibility of preparing the membrane material. WJ provides nutritional support, avoids various complications, and realizes the reuse of waste resources. Our G-E-W membrane does not have specific osteogenic factors that optimize the material selection from the aspects of economic benefits and other side effects [71] such as ectopic osteogenesis or rapid release of factors.

Our membrane-like 3D scaffold has high hydrophilicity and cell compatibility, and a pore structure that is conducive to cell adhesion and
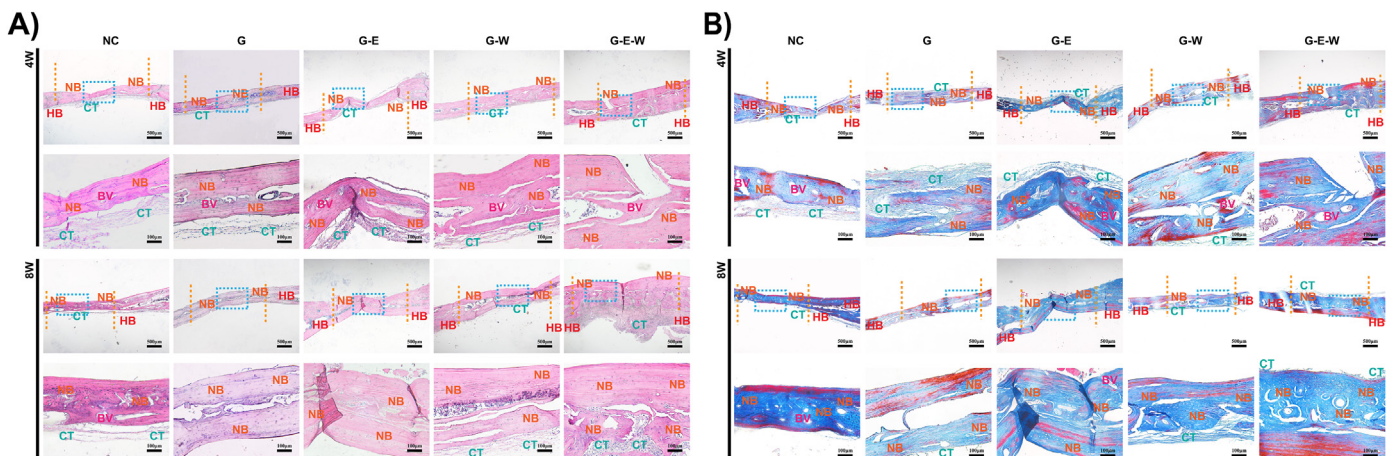

Fig. 9. Histological assessment of bone defect repair using the G, G-E, G-W and G-E-W artificial membranes at 4 and 8 weeks. A) H&E and B)Masson staining of the bone defect repair. BV, blood vessels; CT, connective tissue; G, GelMA membrane; G-E, GelMA-E7membrane; G-W, GelMA-WJMA membrane; G-E-W, GelMA-E7-WJMA membrane; HB, host bone; NB, new bone; NC, negative control.
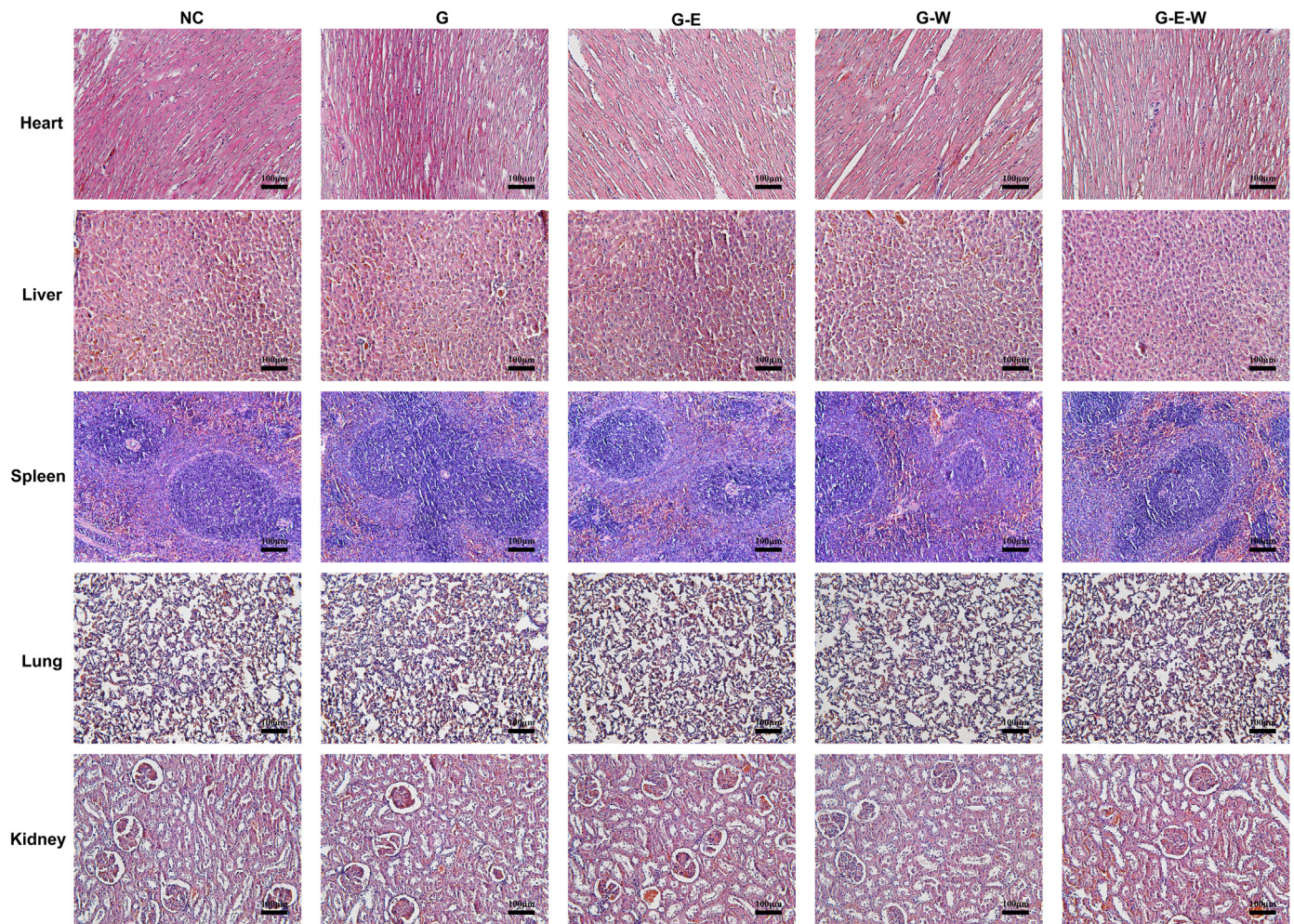
Fig. 10. Histological assessment of important organs in rats with bone defects after 8 weeks using membrane materials. G, GelMA membrane; G-E, GelMA-E7membrane; G-W, GelMA-WJMA membrane; G-E-W, GelMA-E7-WJMA membrane; NC, negative control.

aggregation. The addition of E7 peptide and WJ effectively recruits and anchor MSCs, promotes the osteogenic differentiation of tissues through various growth factors, and strengthens and promotes the mineralization process of bone tissues. The G-E-W membrane prepared in this paper is intended to realize biomimetic reconstruction of a mechanically degradable structure of the periosteum, and also strives for the biomimetic reconstruction of periosteum ECM. At the same time, it is necessary to achieve in situ tissue engineering reconstruction of regenerated cells. On the basis of the extensibility and affinity of this membrane, we aim to realize a multi-layer construction using the G-E-W membrane, and simulate the advantages of natural periosteum in function and structure.

4. Conclusion

In this study, GelMA, E7 peptide, and WJ crosslinked by MA were used to prepare a BCN structural membrane of G-E-W by photo-crosslinking as an artificial periosteum material for bone tissue engineering. The membrane material maintains the mechanical properties and biocompatibility of GelMA, as well as the biological activity of WJ. Moreover, E7 peptide amplifies the role of the membrane materials in the recruitment and proliferation of MSCs. In addition to these advantages, the composite membrane material can stably simulate ECM and promote cell proliferation and osteogenic differentiation, especially for BMSCs. The material can also promote COL deposition and the formation of bone minerals to accelerate the osteogenic differentiation of tissues, and increase the early osteogenesis of fractures and bone defects.

Ethics approval and consent to participate

The authors declare that all animal experiments are approved by the Institutional Animal Care and Use Committee (ZJU20160455) as well as the ARRIVE Guidelines. All authors comply with all relevant ethical regulations.

Credit author statement

WTZ: Conceptualization, Methodology, Software, Formal analysis, Writing - Original Draft. **TZS:** Methodology, Software, Formal analysis, Writing - Review & Editing. **JZ:** Software, Validation, Visualization, Project administration. **XTH:** Methodology, Investigation, Visualization. **MY:** Validation, Investigation, Data Curation. **LWH:** Methodology, Investigation, Data Curation, Project administration. **GX:** Formal analysis, Resources, Data Curation, Supervision. **YTZ:** Conceptualization, Resources, Supervision. **ZHL:** Conceptualization, Resources, Writing - Review & Editing. **WTZ** and **TZS** contributed equally to the manuscript and should be considered co-first authors.

Funding

Declaration of competing interest

The authors declare that they have no known competing financial interests or personal relationships that could have appeared to influence the work reported in this paper.

Data availability

Data will be made available on request.

Acknowledgments

References

[1] D. Marsh, Concepts of fracture union, delayed union, and nonunion, Clin. Orthop. Relat. Res. (355 Suppl) (1998) S22–S30.
[2] J. Zhu, Y. Liu, C. Chen, H. Chen, J. Huang, Y. Luo, et al., Cyasterone accelerates fracture healing by promoting MSCs migration and osteogenesis, J Orthop Translat 28 (2021) 28–38.
[3] A. Bharadwaz, A.C. Jayasuriya, Recent trends in the application of widely used natural and synthetic polymer nanocomposites in bone tissue regeneration, Mater Sci Eng C Mater Biol Appl 110 (2020), 110698.
[4] B. Wang, J. Liu, D. Niu, N. Wu, W. Yun, W. Wang, et al., Mussel-inspired bisphosphonated injectable nanocomposite hydrogels with adhesive, self-healing, and osteogenic properties for bone regeneration, ACS Appl. Mater. Interfaces 13 (28) (2021) 32673–32689.
[5] X. Zhang, H.A. Awad, R.J. O'Keefe, R.E. Guldberg, E.M. Schwarz, A perspective: engineering periosteum for structural bone graft healing, Clin. Orthop. Relat. Res. 466 (8) (2008) 1777–1787.
[6] K. Zhang, Z. Jia, B. Yang, Q. Feng, X. Xu, W. Yuan, et al., Adaptable hydrogels mediate cofactor-assisted activation of biomarker-responsive drug delivery via positive feedback for enhanced tissue regeneration, Adv. Sci. 5 (12) (2018), 1800875.
[7] I.A. Urban, A. Monje, Guided bone regeneration in alveolar bone reconstruction, Oral Maxillofac. Surg. Clin. 31 (2) (2019) 331–338.
[8] X. Lin, C. Zhao, P. Zhu, J. Chen, H. Yu, Y. Cai, et al., Periosteum extracellular-matrix-mediated acellular mineralization during bone formation, Adv Healthc Mater 7 (4) (2018).
[9] G. Yang, H. Liu, Y. Cui, J. Li, X. Zhou, N. Wang, et al., Bioinspired membrane provides periosteum-mimetic microenvironment for accelerating vascularized bone regeneration, Biomaterials 268 (2021) 120561.
[10] W. Zhang, N. Wang, M. Yang, T. Sun, J. Zhang, Y. Zhao, et al., Periosteum and development of the tissue-engineered periosteum for guided bone regeneration, J Orthop Translat 33 (2022) 41–54.
[11] F. Nitzsche, C. Müller, B. Lukomska, J. Jolkkonen, A. Deten, J. Boltze, Concise Review: MSC adhesion cascade-insights into homing and transendothelial migration, Stem Cell. 35 (6) (2017) 1446–1460.
[12] S. Chin, K.I. Furukawa, K. Kurotaki, N. Nagasaki, K. Wada, G. Kumagai, et al., Facilitation of chemotaxis activity of mesenchymal stem cells via stromal cell-derived factor-1 and its receptor may promote ectopic ossification of human spinal ligaments, J. Pharmacol. Exp. Therapeut. 369 (1) (2019) 1–8.
[13] N.M. Moll, R.M. Ransohoff, CXCL12 and CXCR4 in bone marrow physiology, Expet Rev. Hematol. 3 (3) (2010) 315–322.
[14] T.S. Fu, Y.C. Wang, C.H. Chen, C.W. Chang, T.Y. Lin, C.B. Wong, et al., Engineered periosteum-bone biomimetic bone graft enhances posterolateral spine fusion in a rabbit model, Spine J. 19 (4) (2019) 762–771.
[15] L. Zhao, J. Zhao, Z. Tuo, G. Ren, Repair of long bone defects of large size using a tissue-engineered periosteum in a rabbit model, J. Mater. Sci. Mater. Med. 32 (9) (2021) 105.
[16] J. He, Z. Li, T. Yu, W. Wang, M. Tao, S. Wang, et al., In vitro and in vivo biocompatibility study on acellular sheep periosteum for guided bone regeneration, Biomed. Mater. 15 (1) (2020), 015013.
[17] Y. Lou, H. Wang, G. Ye, Y. Li, C. Liu, M. Yu, et al., Periosteal tissue engineering: current developments and perspectives, Adv Healthc Mater 10 (12) (2021), e2100215.
[18] Y. Yang, T. Xu, Q. Zhang, Y. Piao, H.P. Bei, X. Zhao, Biomimetic, stiff, and adhesive periosteum with osteogenic-angiogenic coupling effect for bone regeneration, Small 17 (14) (2021), e2006598.
[19] L. Laijun, Z. Yu, L. Chaojing, M. Jifu, W. Fujun, W. Lu, An enhanced periosteum structure/function dual mimicking membrane for in-situ restorations of periosteum and bone, Biofabrication 13 (3) (2021).
[20] W. Liu, W. Bi, Y. Sun, L. Wang, X. Yu, R. Cheng, et al., Biomimetic organic-inorganic hybrid hydrogel electrospinning periosteum for accelerating bone regeneration, Mater Sci Eng C Mater Biol Appl 110 (2020), 110670.
[21] T. Xin, Y. Gu, R. Cheng, J. Tang, Z. Sun, W. Cui, et al., Inorganic strengthened hydrogel membrane as regenerative periosteum, ACS Appl. Mater. Interfaces 9 (47) (2017) 41168–41180.
[22] N. Celikkin, S. Mastrogiacomo, J. Jaroszewicz, X.F. Walboomers, W. Swieszkowski, Gelatin methacrylate scaffold for bone tissue engineering: the influence of polymer concentration, J. Biomed. Mater. Res. 106 (1) (2018) 201–209.
[23] I. Ullah, Z. Hussain, Y. Zhang, X. Liu, S. Ullah, Y. Zhang, et al., Inorganic nanomaterial-reinforced hydrogel membrane as an artificial periosteum, Appl. Mater. Today 28 (2022), 101532.
[24] Y. Yang, T. Xu, Q. Zhang, Y. Piao, H.P. Bei, X. Zhao, Biomimetic, stiff, and adhesive periosteum with osteogenic–angiogenic coupling effect for bone regeneration, Small 17 (14) (2021), 2006598.
[25] K. Sobolewski, E. Bańkowski, L. Chyczewski, S. Jaworski, Collagen and glycosaminoglycans of Wharton's jelly, Biol. Neonate 71 (1) (1997) 11–21.
[26] S. Franc, J.C. Rousseau, R. Garrone, M. van der Rest, M. Moradi-Améli, Microfibrillar composition of umbilical cord matrix: characterization of fibrillin, collagen VI and intact collagen V, Placenta 19 (1) (1998) 95–104.
[27] K. Sobolewski, A. Małkowski, E. Bańkowski, S. Jaworski, Wharton's jelly as a reservoir of peptide growth factors, Placenta 26 (10) (2005) 747–752.
[28] B. Beiki, B. Zeynali, E. Seyedjafari, Fabrication of a three dimensional spongy scaffold using human Wharton's jelly derived extra cellular matrix for wound healing, Mater Sci Eng C Mater Biol Appl 78 (2017) 627–638.
[29] N. Forraz, C.P. McGuckin, The umbilical cord: a rich and ethical stem cell source to advance regenerative medicine, Cell Prolif 44 (Suppl 1) (2011) 60–69. Suppl 1.
[30] T. Li, M. Xia, Y. Gao, Y. Chen, Y. Xu, Human umbilical cord mesenchymal stem cells: an overview of their potential in cell-based therapy, Expet Opin. Biol. Ther. 15 (9) (2015) 1293–1306.
[31] Y.J. Cai, L. Huang, T.Y. Leung, A. Burd, A study of the immune properties of human umbilical cord lining epithelial cells, Cytotherapy 16 (5) (2014) 631–639.
[32] M.L. Weiss, C. Anderson, S. Medicetty, K.B. Seshareddy, R.J. Weiss, I. VanderWerff, et al., Immune properties of human umbilical cord Wharton's jelly-derived cells, Stem Cell. 26 (11) (2008) 2865–2874.
[33] Z. Shao, X. Zhang, Y. Pi, X. Wang, Z. Jia, J. Zhu, et al., Polycaprolactone electrospun mesh conjugated with an MSC affinity peptide for MSC homing in vivo, Biomaterials 33 (12) (2012) 3375–3387.
[34] L. Wang, N. Wang, W. Zhang, X. Cheng, Z. Yan, G. Shao, et al., Therapeutic peptides: current applications and future directions, Signal Transduct. Targeted Ther. 7 (1) (2022) 1–27.
[35] J. Wu, L. Cao, Y. Liu, A. Zheng, D. Jiao, D. Zeng, et al., Functionalization of silk fibroin electrospun scaffolds via BMSC affinity peptide grafting through oxidative self-polymerization of dopamine for bone regeneration, ACS Appl. Mater. Interfaces 11 (9) (2019) 8878–8895.
[36] W. Zhang, C. Ling, A. Zhang, H. Liu, Y. Jiang, X. Li, et al., An all-silk-derived functional nanosphere matrix for sequential biomolecule delivery and in situ osteochondral regeneration, Bioact. Mater. 5 (4) (2020) 832–843.
[37] X. Zheng, X. Pan, Q. Pang, C. Shuai, L. Ma, C. Gao, Selective capture of mesenchymal stem cells over fibroblasts and immune cells on E7-modified collagen substrates under flow circumstances, J. Mater. Chem. B 6 (1) (2018) 165–173.
[38] B.K. Culpepper, M.C. Phipps, P.P. Bonvallet, S.L. Bellis, Enhancement of peptide coupling to hydroxyapatite and implant osseointegration through collagen mimetic peptide modified with a polyglutamate domain, Biomaterials 31 (36) (2010) 9586–9594.
[39] B.K. Culpepper, P.P. Bonvallet, M.S. Reddy, S. Ponnazhagan, S.L. Bellis, Polyglutamate directed coupling of bioactive peptides for the delivery of osteoinductive signals on allograft bone, Biomaterials 34 (5) (2013) 1506–1513.
[40] L. Liu, Y. Shang, C. Li, Y. Jiao, Y. Qiu, C. Wang, et al., Hierarchical nanostructured electrospun membrane with periosteum-mimic microenvironment for enhanced bone regeneration, Adv Healthc Mater 10 (21) (2021), e2101195.
[41] Q. Zhang, C. Chang, C. Qian, W. Xiao, H. Zhu, J. Guo, et al., Photo-crosslinkable amniotic membrane hydrogel for skin defect healing, Acta Biomater. 125 (2021) 197–207.
[42] M. Gholipourmalekabadi, A. Samadikuchaksaraei, A.M. Seifalian, A.M. Urbanska, H. Ghanbarian, J.G. Hardy, et al., Silk fibroin/amniotic membrane 3D bi-layered artificial skin, Biomed. Mater. 13 (3) (2018), 035003.
[43] Q. Zhang, C. Qian, W. Xiao, H. Zhu, J. Guo, Z. Ge, et al., Development of a visible light, cross-linked GelMA hydrogel containing decellularized human amniotic particles as a soft tissue replacement for oral mucosa repair, RSC Adv. 9 (32) (2019) 18344–18352.
[44] D.H. Ma, J.Y. Lai, H.Y. Cheng, C.C. Tsai, L.K. Yeh, Carbodiimide cross-linked amniotic membranes for cultivation of limbal epithelial cells, Biomaterials 31 (25) (2010) 6647–6658.
[45] P.P. Spicer, J.D. Kretlow, S. Young, J.A. Jansen, F.K. Kasper, A.G. Mikos, Evaluation of bone regeneration using the rat critical size calvarial defect, Nat. Protoc. 7 (10) (2012) 1918–1929.
[46] R. Gao, M. Watson, K.E. Callon, M. Tuari, M. Dray, D. Naot, et al., Local application of lactoferrin promotes bone regeneration in a rat critical-sized calvarial defect model as demonstrated by micro-CT and histological analysis, J Tissue Eng Regen Med 12 (1) (2018) e620–e626.
[47] C. Klein, M. Monet, V. Barbier, A. Vanlaeys, A.C. Masquelet, R. Gouron, et al., The Masquelet technique: current concepts, animal models, and perspectives, J Tissue Eng Regen Med 14 (9) (2020) 1349–1359.
[48] Z. Ghaffarinovin, O. Soltaninia, Y. Mortazavi, A. Esmaeilzadeh, S. Nadri, Repair of rat cranial bone defect by using amniotic fluid-derived mesenchymal stem cells in

polycaprolactone fibrous scaffolds and platelet-rich plasma, Bioimpacts 11 (3) (2021) 209–217.

[49] W. Kim, H. Lee, J. Lee, A. Atala, J.J. Yoo, S.J. Lee, et al., Efficient myotube formation in 3D bioprinted tissue construct by biochemical and topographical cues, Biomaterials 230 (2020), 119632.

[50] G. Eke, N. Mangir, N. Hasirci, S. MacNeil, V. Hasirci, Development of a UV crosslinked biodegradable hydrogel containing adipose derived stem cells to promote vascularization for skin wounds and tissue engineering, Biomaterials 129 (2017) 188–198.

[51] M.A. Sherman, J.P. Kennedy, D.L. Ely, D. Smith, Novel polyisobutylene/ polydimethylsiloxane bicomponent networks: III. Tissue compatibility, J. Biomater. Sci. Polym. Ed. 10 (3) (1999) 259–269.

[52] G. Vunjak-Novakovic, L.E. Freed, Culture of organized cell communities, Adv. Drug Deliv. Rev. 33 (1–2) (1998) 15–30.

[53] X. Sun, Q. Lang, H. Zhang, L. Cheng, Y. Zhang, G. Pan, et al., Electrospun photocrosslinkable hydrogel fibrous scaffolds for rapid in vivo vascularized skin flap regeneration, Adv. Funct. Mater. 27 (2) (2017), 1604617.

[54] S.H. McBride, S.F. Evans, M.L. Knothe Tate, Anisotropic mechanical properties of ovine femoral periosteum and the effects of cryopreservation, J. Biomech. 44 (10) (2011) 1954–1959.

[55] O.Z. Fisher, A. Khademhosseini, R. Langer, N.A. Peppas, Bioinspired materials for controlling stem cell fate, Acc. Chem. Res. 43 (3) (2010) 419–428.

[56] W. Schuurman, P.A. Levett, M.W. Pot, P.R. van Weeren, W.J. Dhert, D.W. Hutmacher, et al., Gelatin-methacrylamide hydrogels as potential biomaterials for fabrication of tissue-engineered cartilage constructs, Macromol. Biosci. 13 (5) (2013) 551–561.

[57] J.W. Nichol, S.T. Koshy, H. Bae, C.M. Hwang, S. Yamanlar, A. Khademhosseini, Cell-laden microengineered gelatin methacrylate hydrogels, Biomaterials 31 (21) (2010) 5536–5544.

[58] Z. Shao, X. Zhang, Y. Pi, X. Wang, Z. Jia, J. Zhu, et al., Polycaprolactone electrospun mesh conjugated with an MSC affinity peptide for MSC homing in vivo, Biomaterials 33 (12) (2012) 3375–3387.

[59] Q. Li, D. Xing, L. Ma, C. Gao, Synthesis of E7 peptide-modified biodegradable polyester with the improving affinity to mesenchymal stem cells, Mater Sci Eng C Mater Biol Appl 73 (2017) 562–568.

[60] N. Bakhtyar, M.G. Jeschke, E. Herer, M. Sheikholeslam, S. Amini-Nik, Exosomes from acellular Wharton's jelly of the human umbilical cord promotes skin wound healing, Stem Cell Res. Ther. 9 (1) (2018) 193.

[61] B. Heissig, K. Hattori, S. Dias, M. Friedrich, B. Ferris, N.R. Hackett, et al., Recruitment of stem and progenitor cells from the bone marrow niche requires MMP-9 mediated release of kit-ligand, Cell 109 (5) (2002) 625–637.

[62] M. Agathocleous, W.A. Harris, Metabolism in physiological cell proliferation and differentiation, Trends Cell Biol. 23 (10) (2013) 484–492.

[63] R. Marom, I. Shur, R. Solomon, D. Benayahu, Characterization of adhesion and differentiation markers of osteogenic marrow stromal cells, J. Cell. Physiol. 202 (1) (2005) 41–48.

[64] S. Kim, C. Cha, Enhanced mechanical and electrical properties of heteroscaled hydrogels infused with aqueous-dispersible hybrid nanofibers, Biofabrication 12 (1) (2019), 015020.

[65] M. Zaborowska, A. Bodin, H. Bäckdahl, J. Popp, A. Goldstein, P. Gatenholm, Microporous bacterial cellulose as a potential scaffold for bone regeneration, Acta Biomater. 6 (7) (2010) 2540–2547.

[66] Q. Feng, J. Xu, K. Zhang, H. Yao, N. Zheng, L. Zheng, et al., Dynamic and cell-infiltratable hydrogels as injectable carrier of therapeutic cells and drugs for treating challenging bone defects, ACS Cent. Sci. 5 (3) (2019) 440–450.

[67] Y. Watanabe, N. Harada, K. Sato, S. Abe, K. Yamanaka, T. Matushita, Stem cell therapy: is there a future for reconstruction of large bone defects? Injury 47 (Suppl 1) (2016) S47–S51.

[68] S. Kargozar, R.K. Singh, H.W. Kim, F. Baino, Hard" ceramics for "Soft" tissue engineering: paradox or opportunity? Acta Biomater. 115 (2020) 1–28.

[69] Z. Yang, Z. Yang, L. Ding, P. Zhang, C. Liu, D. Chen, et al., Self-adhesive hydrogel biomimetic periosteum to promote critical-size bone defect repair via synergistic osteogenesis and angiogenesis, ACS Appl. Mater. Interfaces 14 (32) (2022) 36395–36410.

[70] Y. Yu, Y. Wang, W. Zhang, H. Wang, J. Li, L. Pan, et al., Biomimetic periosteum-bone substitute composed of preosteoblast-derived matrix and hydrogel for large segmental bone defect repair, Acta Biomater. 113 (2020) 317–327.

[71] A.W. James, G. LaChaud, J. Shen, G. Asatrian, V. Nguyen, X. Zhang, et al., A Review of the clinical side effects of bone morphogenetic protein-2, Tissue Eng. B Rev. 22 (4) (2016) 284–297.